Am J Cancer Res 2024;14(8):3665-3693
www.ajcr.us /ISSN:2156-6976/ajcr0155153

Original Article

Integrative analysis of autophagy-related genes reveals that CAPNS1 is a novel prognostic biomarker and promotes the malignancy of melanoma via Notch signaling pathway

Mengru Gao[1,2], Jisong Liu[3], Miaomiao Yang[1,2], Xiangzhou Zhang[3], Yulian Zhang[1,2], Zhuliang Zhou[3], Jiabin Deng[3]

[1]Clinical Pathology Center, The First Affiliated Hospital of Anhui Medical University, Hefei 230012, Anhui, China; [2]Anhui Public Health Clinical Center, Hefei 230012, Anhui, China; [3]Department of Burn and Plastic Surgery, The Third People's Hospital of Bengbu, Bengshan District, Bengbu 233000, Anhui, China

Received December 28, 2023; Accepted July 15, 2024; Epub August 25, 2024; Published August 30, 2024

Abstract: Skin cutaneous melanoma (SKCM) is a highly fatal form of skin cancer that develops from the malignant transformation of epidermal melanocytes. There is substantial evidence linking autophagy to cancer etiology and immunotherapy efficacy. This study aimed to conduct a comprehensive analysis of autophagy-related genes (ARGs) using TCGA datasets and further explore the potential function of critical ARGs in SKCM progression. We performed comprehensive bioinformatics analysis uses the TCGA dataset. RT-PCR was applied to examine the expression of CAPNS1 in SKCM cells. Lost-of-function experiments were performed to detect the expression of the related proteins. In this search, we screed 70 differentially expressed autophagy-related genes (DE-ARGs), including 33 up-DE-ARGs and 37 down-DE-ARGs. Enrichment assays revealed that these 70 DE-ARGs may exert influence on critical cellular processes such as autophagy, protein kinase activity, and signaling pathways, impacting cell growth, differentiation, survival, and tumor development. Then, we further explore the prognostic value of 70 DE-ARGs and confirmed 18 survival-related DE-ARGs in SKCM patients. Nearly all the 18 DE-ARGs' methylation was negatively correlated with their corresponding expression in SKCM. The 12 survival-related DE-ARGs were used to develop a unique predictive model that effectively classified SKCM patients into high- and low-risk groups with regard to overall survival. Furthermore, tumor environment analysis indicated that the risk score was associated with several immune cells. Among the 12 survival-related DE-ARGs, our attention focused on CAPNS1 which was highly expressed in SKCM patients and predicted a poor prognosis. In addition, we confirmed that knockdown of CAPNS1 distinctly suppressed the proliferation, metastasis and EMT of SKCM cells, and promoted autophagy via regulating Notch signaling pathway. Overall, this study enhances our understanding of the intricate molecular landscape of SKCM progression and presents promising avenues for future research and clinical applications.

Keywords: Skin cutaneous melanoma, CAPNS1, immune microenvironment, autophagy, biomarker, prognosis signature, Notch signaling pathway

Introduction

Skin Cutaneous Melanoma (SKCM) is a type of skin cancer, which originates from the malignant transformation of epidermal melanocytes, with high lethality [1]. The incidence of SKCM varies globally, with higher rates typically observed in regions with intense ultraviolet (UV) radiation, such as Australia, New Zealand, South Africa, and certain areas of the United States [2]. This association is linked to the fact that UV exposure is a major environmental risk factor for SKCM. SKCM is more common in Caucasian individuals, particularly those with fair skin. Asians and Black individuals have a relatively lower risk of developing melanoma, but there has been a growing trend of increasing incidence in some regions in recent years. SKCM typically occurs in adulthood, but it can also affect children and adolescents. Age is an important risk factor, and as age increases, the risk of developing melanoma gradually rises.

https://doi.org/10.62347/ECDF2762

Individuals with suppressed immune systems, such as those who undergo organ transplant and require immunosuppressive medications, have a higher risk of developing melanoma [3, 4]. The breakthrough advancements in targeted treatment and immunotherapy have drastically improved the prognosis of melanoma patients. However, the efficacy of existing medicines has been severely impeded by tumor cell heterogeneity-induced difficulties in identifying treatment resistance, low response rates and susceptible subpopulations [5, 6]. The biggest difficulty in therapeutic therapy of SKCM is the lack of clarity around its pathophysiology. Consequently, it is crucial to find innovative biomarkers for SKCM diagnosis and individualized therapy.

Autophagy is a highly regulated cellular process that involves the encapsulation of cellular waste, damaged organelles, and excess proteins into membrane-bound vesicles [7]. These vesicles, known as autophagosomes, are subsequently transported to lysosomes for degradation and recycling. The regulation of this process involves a series of genes and signaling pathways, including the participation of proteins such as Beclin-1, Atg5, Atg7, and Atg8 [8, 9]. The process of autophagy is extremely important to the upkeep of cellular homeostasis as well as cellular survival. It helps cells adapt to changing environmental conditions, such as starvation, by breaking down cellular components to obtain energy and essential metabolites [10]. Additionally, autophagy is involved in cell differentiation and organ development, contributing to the regulation of cellular fate and function. In the context of diseases, autophagy dysfunction is associated with a variety of conditions [11, 12]. For instance, impaired autophagy can lead to the accumulation of aberrant proteins, contributing to neurodegenerative disorders like Parkinson's and Alzheimer's diseases. On the other hand, some tumors may suppress autophagy to gain a survival advantage. Furthermore, autophagy can influence immune responses, playing a role in autoimmune diseases and infections. Exploring the intricate mechanisms of autophagy is crucial for uncovering the mysteries of cellular biology and developing therapeutic approaches for autophagy-related diseases. Consequently, understanding autophagy regulation, signaling pathways, and crosstalk with other cellular processes provides a fresh perspective on comprehending cellular equilibrium, disease pathogenesis, and innovative treatment strategies [13, 14]. To date, the potential function of autophagy-related genes (ARGs) in the progression of Melanoma remained largely unclear.

High-Throughput Sequencing, also known as Next-Generation Sequencing (NGS), is a revolutionary DNA and RNA analysis technology characterized by its speed, efficiency, and accuracy [15]. Compared to traditional Sanger sequencing methods, high-throughput sequencing has made significant breakthroughs in terms of throughput, speed, and cost, enabling unprecedented possibilities for large-scale genome and transcriptome research [16]. High-throughput sequencing involves various technology platforms, such as Illumina, Ion Torrent, PacBio, and Oxford Nanopore. Despite differences in technical principles, the basic workflow includes key steps like library preparation, amplification, sequencing, and data analysis [17, 18]. In the library preparation stage, DNA or RNA samples are prepared into libraries suitable for sequencing. The amplification stage enhances signal intensity through methods like PCR. During sequencing, diverse platforms are used to sequence library fragments on a large scale. The final data analysis transforms raw sequencing data into meaningful biological information, such as genomic variations and gene expression levels. High-throughput sequencing plays a pivotal role in cancer research by providing profound insights into the molecular mechanisms underlying tumor development and progression [19, 20]. This technological innovation equips researchers with a powerful toolset to comprehensively, efficiently, and accurately analyze genetic variations, gene expression abnormalities, and molecular features associated with tumor development. One of the key roles of high-throughput sequencing in cancer research is the analysis of genomic variations. Through comprehensive genome sequencing, we can identify mutations, insertions, deletions, and other variations that help pinpoint critical genes involved in tumor initiation and suppression. This aids in identifying new therapeutic targets and developing personalized treatment strategies. Moreover, high-throughput sequencing is crucial in the field of cancer genomics. It allows us to deeply sequence the entire cancer genome,

facilitating a better understanding of the genetic characteristics of cancer and providing essential information for the development of precision medicine [21, 22]. In transcriptomics research, high-throughput sequencing reveals the gene expression profiles within tumor cells, assisting in uncovering molecular features and potential therapeutic targets. Additionally, by analyzing epigenetic marks such as DNA methylation and histone modifications, high-throughput sequencing unveils the associations between tumor development and epigenetic changes. High-throughput sequencing also plays a role in studying tumor microbiomics, shedding light on the interactions between microorganisms and tumors, along with their potential impacts.

The objective of this study is to conduct a comprehensive analysis of TCGA dataset, aiming to provide an extensive depiction of the expression profiles of autophagy-related genes and their association with prognosis. Through systematic data mining and bioinformatics analysis, our intention is to identify key genes that play crucial roles in the development and progression of melanoma. By delving into the functionality and regulatory networks of these pivotal genes, our goal is to elucidate their potential roles in governing essential processes such as autophagy regulation, cell proliferation, metastasis, and the formation of the tumor microenvironment. Ultimately, our study aims to offer profound insights, uncovering the pivotal role of autophagy in melanoma development and providing novel possibilities for the identification of therapeutic targets and precision medicine approaches. Through comprehensive analysis of autophagy regulatory networks and functional validation of key genes, we will gain a deeper understanding of the molecular mechanisms underlying melanoma and establish crucial scientific foundations for the development of innovative therapeutic strategies.

Mehods and materials

Cell lines and cell culture

HEMa-LP cell line (a human keratinocyte cell line, as control cells) and human melanoma cell lines including SK-MEL-24, A-375 and SK-MEL-1 cell lines were obtained from the American Type Culture Collection (ATCC; Manassas, VA, USA). Another two human melanoma cell lines including SK-MEL-28 and A2058 cell lines were purchased from Shanghai Cell Bank (Xuhui, Shanghai, China). The cells were cultured in RPMI-1640 media (Excell, Taicang, Jiangsu, China) containing 10% FBS (Gibco, Carlsbad, CA, USA), 2000 U/ml penicillin G (1,000,000 U = 1 g; Shenggong Biotech, Songjiang, Shanghai, China) and 500 μg/ml streptomycin solution (Shenggong Biotech, Songjiang, Shanghai, China). The cells were cultured in a humidified incubator at 37°C and 5% CO_2.

Cell transfection

In the present study, the siRNAs were used to knockdown CAPNS1 (si-CAPNS1#1, si-CAPNS1#2), and these siRNAs including si-Control siRNAs were synthesized by Shenggong Biotech company (Songjiang, Shanghai, China). For cell transfection, Lipofectamine 3000 reagent kits (Thermo Fisher Scientific, Inc., Waltham, MA, USA) were employed, and the siRNA transfection was conducted in accordance with the kits' protocols. In brief, the siRNAs and Lipofectamine 3000 reagent were diluted with Opti-MEM (Gibco, Carlsbad, CA, USA). Then, the melanoma cells were placed into 96-well plates and when the cells reached about 70% confluence, 20 pmol siRNAs (si-Control, si-CAPNS1#1, or si-CAPNS1#2) were respectively mixed with Lipofectamine 3000 reagent. Afterwards, following an incubation period of five minutes at room temperature for the combination, the components were then inserted into the cells. After five hours, the medium was discarded, and after forty-eight hours, the cells were put to use in the tests.

CCK-8 assays

Cell growth assays were performed by using CCK-8 kits from Beyotime Biotechnology company (Haimen, Jiangsu, China). In brief, 3×10^3 cells (per well) after siRNAs transfection were seeded into 96-well plates and cultivated in DMEM containing 10% FBS for cell attachment. Subsequently, CCK-8 reagents (10 μl) was added to each well, and the cells were continue to culture for 2 hours. After that, the absorbance at 450 nm (OD 450 nm) was measured at each of the given time points (24, 48, 72, and 96 hours) using a microplate reader.

Ethynyl deoxyuridine (EdU) incorporation assays

The cell proliferation after various treatment was evaluated by the EdU incorporation assays via using EdU assay kits from Beyotime Biotechnology company (Haimen, Jiangsu, China). In brief, following siRNAs transfection, 2 × 10^3 cells were seeded into each well of a 96-well plate, and the plates were then cultured with EdU reagent at a 1:1000 dilution for two hours. Then, 4% paraformaldehyde (PFA; Shenggong, Songjiang, Shanghai, China) was used to fix the cells, followed by treating with Triton X-100 solution. Afterwards, the cells were incubated with the 1× Apollo reaction cocktail for 30 min and DAPI reagent staining for 10 min. The fluorescence of the cells were then visualized by using a fluorescence microscope.

Total RNA isolation and real-time PCR assays

Total RNAs from melanoma cells after siRNAs (si-Control, si-CAPNS1#1, or si-CAPNS1#2) transfection were extracted by using TRIzol reagent kits (Shenggong, Songjiang, Shanghai, China), and the quantity of the RNA was determined by NanoDrop ND-1000 spectrophotometer (Thermo Fisher Scientific, Inc., Waltham, MA, USA). Afterwards, the cDNA was reverse-transcribed by using first strand cDNA synthesis kits (Thermo Fisher Scientific, Inc., Waltham, MA, USA). Then, real-time PCR assays for CAPNS1 examination were performed by using TAKARA SYBR Premix Ex Taq real-time PCR kits (Dalian, Liaoning, China). The reference gene used in the present study was GAPDH. Relative CAPNS1 expression was calculated using the $2^{-\Delta\Delta Ct}$ method. The primers for CAPNS1 and GAPDH were listed as following: F-CAPNS1: 5'-GACACCCTGATCTGAAGACTGA-3'; R-CAPNS1: 5'-GCCTGCCACCTTTTGATGTT-3'; F-GAPDH: 5'-CCACATCGCTCAGACACCAT-3'; R-GAPDH: 5'-ACCAGGCGCCCAATACG-3'.

Transwell assay

The 24-well-8-m transwell chamber (Thermo Fisher Scientific) was used to measure the invasion of A-375 and SK-MEL-28 cells. 5 × 10^4 transfected cells were put into each well of a 24-well plate. Matrigel (BD Biosciences, San Jose, California, USA) was used to line the chambers. The 10% FBS medium was placed in the lower chamber, whereas medium devoid of serum was used to fill the upper chamber. 4% formaldehyde and methanol were used to fix the cells after 48 hours. Under an inverted microscope, invading cells were counted after being scraped off with cotton swabs. The number of invading cells was quantified and analyzed statistically to determine the extent of invasion and compare between experimental conditions or cell lines. Statistical analysis was performed using appropriate software, and results were presented graphically.

Wound healing assay

Cells were plated at a density of 3 × 10^5/well in 6-well plates and allowed to reach 80-90% confluence. Pipette tips were used to scratch parallel lines in the monolayer, and serum-free media was used to keep the cells alive. At 0, 12, 24, and 48 hours, wounds were examined under an inverted microscope to check on their progress. The rate of cell migration was calculated as the proportional increase or decrease in wound width. ImageJ was used to examine the data.

Immunofluorescence

Coverslips containing 7.5 × 10^3 SKCM cells were plated in 24-well plates. Following treatment, the cells were blocked with 5% BSA for 1 hour at room temperature and then fixed in 4% paraformaldehyde for 20 minutes. The cells were then permeabilized with 0.1% Triton X-100 (P0096, Beyotime) for 30 minutes. Next, cells were incubated with primary antibody (1:1000), galectin-3 or LC3B overnight at 4°C and incubated with Alexa Fluor secondary antibody. A confocal microscope was used to examine the cells.

In vivo model

The pathogen-free environment was maintained for the female BALB/c mice, who weighed eighteen to twenty grams, were four to six weeks old, and lived in groups of four. A blinded randomization process was used to divide ten mice into two groups, each consisting of five mice, and then each group was given a separate therapy. Both statistical power and ethical requirements were taken into consideration while determining the size of the sample. Subcutaneous injections of 2.0 × 10^7 A-375 and A-375-sh-CAPNS1 cells administered in

100 μL of PBS were administered to the mice belonging to each group. The First Affiliated Hospital of Anhui Medical University's Institutional Animal Care and Use Committee gave their approval for all animal experiments, which were conducted in accordance with the Guidelines for the Care and Use of Laboratory Animals.

Western blot assays

Total proteins from melanoma cells after siRNAs (si-Control, si-CAPNS1#1, or si-CAPNS1#2) transfection were extracted by using lysis buffer kits for western blot (Solarbio, Beijing, China). After that, the proteins in the cell lysates were separated using SDS-PAGE, and then they were successively transferred to PVDF membranes. After blocking the membranes with 5% BSA in PBS/Tween-20, the membranes were incubated at 4 degrees Celsius with the primary antibody. After 12 hours incubation, the membranes were incubated with corresponding secondary antibodies, following visualized using a super ECL luminescence reagent kits (YEASEN, Shanghai, China). The, N-cadherin, Vimentin, anti-Notch1 and anti-p21 antibodies were all purchased from Cell Signaling Technology Co., Ltd. (Beverly, MA, USA). The anti-Hes1 antibodies were purchased from Abcam (Boston, MA, USA). ProteinTech in Wuhan, Hubei, China was the supplier of the anti-GAPDH antibodies that were used in this study.

Data collection, deferentially expressed genes (DEGs) identification and overlap genes obtainment

The gene expression data and clinical information of SKCM and other cancer types were downloaded from The Cancer Genome Atlas (TCGA) database (https://portal.gdc.cancer.gov/). A total of 233 autophagy-related genes (ARGs) were obtained from The Human Autophagy Database (HADb, http://www.autophagy.lu/index.html). The deferentially expressed genes (DEGs) in SKCM based on TCGA data were analyzed by using R software "limma" package, and *P*-value < 0.05 and |log2(FC)| > 1 were defined as the threshold of DEGs. Since there are no control normal tissue samples in TCGA-SKCM database, we used 1809 normal tissue samples from GTEx (Genotype-Tissue Expression) database (https://gtexportal.org/home/) as control group and the TCGA-SKCM tumor samples are 471. The differentially expressed autophagy-related genes (DE-ARGs) among TCGA-DEGs, and 233 ARGs were acquired by using Venny2.1 (https://bioinfogp.cnb.csic.es/tools/venny/). The volcano map in the presented study were generated by using R package "ggplot".

Online websites for bioinformatics analyses

The gene expression, survivals, genetic changes including SNV and CNV, methylation in SKCM, pan-cancers or normal tissues were analyzed by using the TIMER 2.0 database (http://timer.cistrome.org/), GEPIA database (http://gepia.cancer-pku.cn/), Gene Set Cancer Analysis (GSCA) database (http://bioinfo.life.hust.edu.cn/GSCA/#/), Harmonizome 3.0 database (https://maayanlab.cloud/Harmonizome/). The CAPNS1 protein expression and immunohistochemistry in SKCM were analyzed by using Human protein atlas (HPA, https://www.proteinatlas.org/). The CCLE database (https://portals.broadinstitute.org/ccle) was used for analyzing the CAPNS1 expression in various melanoma cell lines.

The analyses of gene functional enrichment, gene correlation, gene set variation analysis (GSVA) score, gene set enrichment analysis (GSEA), protein-protein interacting (PPI) network

GO (Gene Ontology) analysis and KEGG (Kyoto Encyclopedia of Genes and Genomes) analysis are two commonly used bioinformatics methods for interpreting gene function and pathways, used to analyze the functional characteristics and biological processes of gene sets. These methods are widely employed in gene expression analysis, transcriptomics research, and genomics research. The gene functional analysis included GO and KEGG analysis, which were conducted by using R software package "clusterProfiler". For gene or multi-genes correlation analysis, the gene expression data in SKCM were downloaded from TCGA database and the gene correlation heatmap was displayed by the R software package "ggstatsplot". Gene Set Variation Analysis (GSVA) is a method used for the analysis of gene expression data, aiming to assess the variation of gene sets across different samples or conditions. Gene sets are groups of genes associated with specific biological functions, pathways, or process-

es. The purpose of GSVA is to transform gene expression data into a new matrix where each row represents a gene set, each column represents a sample, and each element in the matrix indicates the activity level of that gene set in the corresponding sample. GSVA score in pan-cancers was analyzed by using Gene Set Cancer Analysis (GSCA) database (http://bioinfo.life.hust.edu.cn/GSCA/#/). Gene Set Enrichment Analysis (GSEA) is a computational method used for the analysis of gene expression data, with the aim of identifying whether gene sets associated with specific biological functions, pathways, or processes are enriched among different experimental conditions. GSEA assesses the enrichment status of gene sets across various samples or conditions by comparing the distribution of gene sets within the entire gene expression profile, rather than focusing solely on individual gene differences. Gene set enrichment analysis (GSEA) was carried out by using R software (v.4.2.2) package "clusterProfiler" via Hiplot Pro website (https://hiplot.com.cn/). The STRING database (https://cn.string-db.org) was used to create the protein-protein interacting (PPI) network.

The immune-related analyses

TIMER 2.0 database (http://timer.cistrome.org/) was employed to analyze the correlation between CAPNS1 expression and multiple immune cell infiltration in pan-cancers based on different immune score algorithms such as TIMER, EPIC, CIBERSORT, XCELL, QUANTSEQ, MCPCOUNTER. The immune networks of gene or multi-genes with various immune cell types were analyzed by R software package "immuneeconv". Besides, the immune checkpoints and immune scores in different molecular subtypes of SKCM was analyzed by using R software package "immuneeconv". The correlation between the prognostic signature and immune infiltration score was analyzed with the R software "ggstatsplot" package. In addition, the R software "ggstatsplot" was also utilized for analyzing the tumor mutation burden (TMB) and microsatellite instability (MSI) in pan-cancers. TMB is a metric used to assess the quantity of mutations in the genome of a tumor. It represents the number or frequency of mutations detected in the genomic DNA of tumor cells. TMB reflects the accumulated mutations in tumor cells and is typically expressed as the count of mutations or as mutations per megabase (mut/Mb), which is a normalized measure.

MSI is a genetic anomaly observed in the genome of tumor cells, typically characterized by the instability of short repetitive sequences called microsatellites within DNA. These microsatellite regions consist of a variable number of repeating base units and are usually stable in normal circumstances. However, defects in DNA replication and repair mechanisms can lead to the instability of these sequences, giving rise to MSI.

Statistical analysis

The statistical analysis was carried out using the SPSS version 16.0 software (SPSS Inc., Chicago). All data points are expressed as the mean ± standard error of the mean (SEM), which provides an estimate of the variability of the sample means. The Student's t-test was utilized to analyze differences between two groups of genes. To assess the differences among multiple groups, a one-way analysis of variance (ANOVA) was employed. ANOVA is a statistical method that enables the comparison of means between three or more groups. This analysis helps to determine if there are any significant differences among the group means, considering both the within-group variability and the between-group variability. The threshold for statistical significance was set at a *P*-value of less than 0.05.

Results

DEGs of SKCM identification and functional enrichment analysis

To investigate the potential target genes which might contribute to essential roles of melanoma, we first attempted to obtain the DEGs of SKCM based on TCGA-SKCM database. Since there are no control normal tissue samples in TCGA-SKCM database, we used 1809 normal tissue samples from GTEx database as control group and the TCGA-SKCM tumor samples are 471. By using R software package "limma", we obtained 2144 up-regulated genes and 2802 down-regulated genes, and these DEGs were displayed in the volcano plot (**Figure 1A**). Then, the functional enrichment analysis was conducted. The KEGG analysis revealed that these

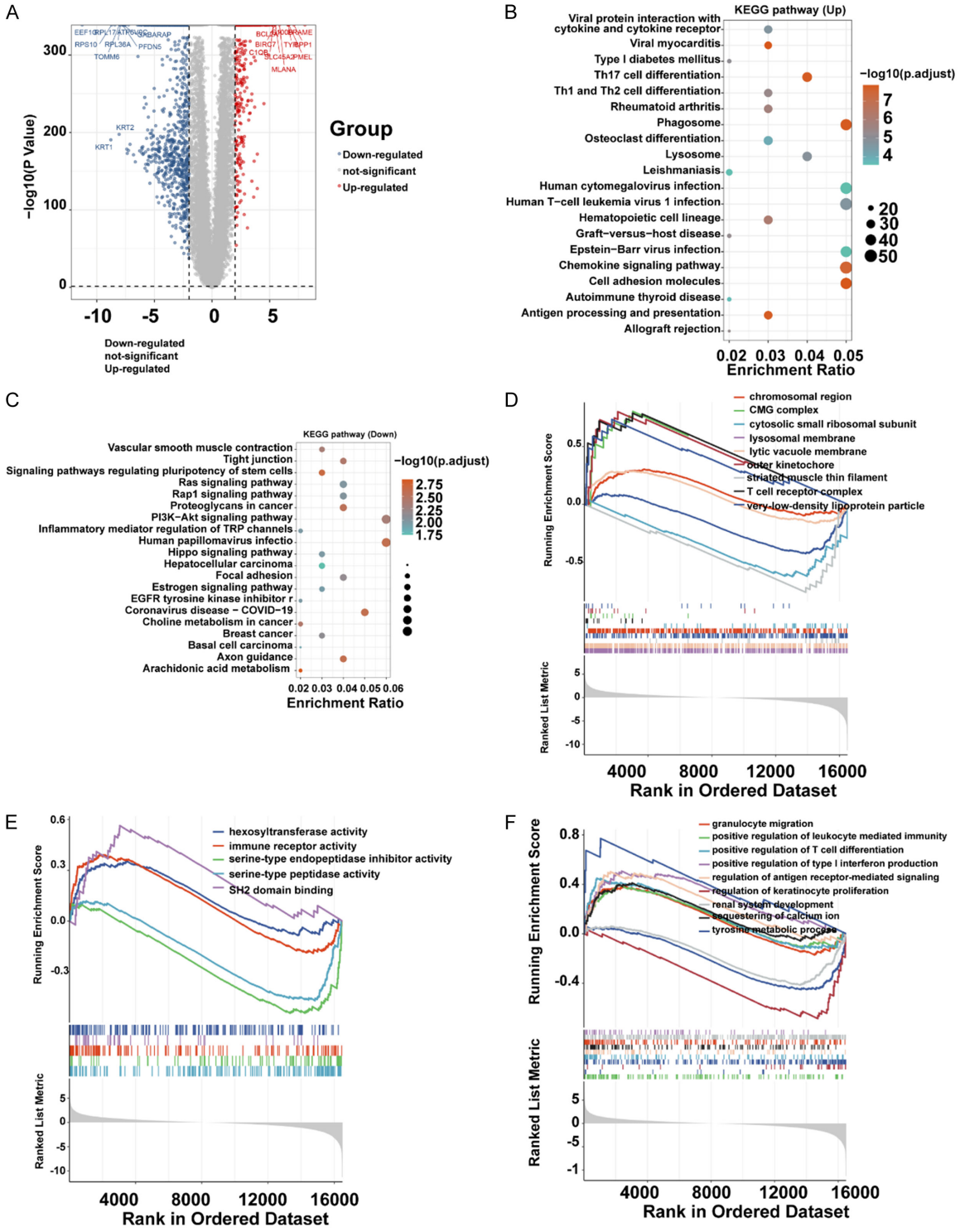

Figure 1. DEGs identification and functional analysis. A. Volcano map. B, C. KEGG analysis of the DEGs. D-F. GSEA of the DEGs in three GO categories.

DEGs were correlated with Viral protein interaction with cytokine and cytokine receptor, Th1 and Th2 cell differentiation, Th17 cell differentiation, Type I diabetes mellitus, Viral myocarditis, PI3K-Akt signaling pathway, Proteoglycans in cancer, Rap1 signaling pathway, Ras signaling pathway, Signaling pathways regulating pluripotency of stem cells, Tight junction and

Vascular smooth muscle contraction, etc. (**Figure 1B** and **1C**). In addition, the GO related GSEA analysis using R software package "clusterProfiler" and "enrichplot", including the biological process (BP), cellular component (CC) and molecular function (MF) categories, were also carried out and displayed in **Figure 1D-F**, respectively, which revealed that these DEGs were mainly enriched in immune cells regulation and enzymes activity.

Clarifying the differentially expressed autophagy-related genes (DE-ARGs) in SKCM

Emerging evidences had demonstrated that autophagy-related genes (ARGs) accounted for crucial roles in regulating cancer development and progression. Therefore, we next sought to clarify the differentially expressed autophagy-related genes (DE-ARGs) in SKCM. To achieve that, the collected 232 ARGs were separately intersected with the above obtained up- or down-regulated genes in SKCM. Consequently, 33 up-DE-ARGs and 37 down-DE-ARGs were obtained, respectively (**Figure 2A**). Afterwards, the 70 total DE-ARGs were subjected to conduct functional enrichment analysis including GO and KEGG analysis. According to the results of GO analysis being displayed by circle interacting plots, the 70 DE-ARGs were mainly enriched in regulation in autophagy, protein kinase activity and ubiquitin (**Figure 2B-D**). Moreover, the KEGG analysis indicated that the 70 DE-ARGs were closely related with Autophagy-animal, Bladder cancer, Chemical carcinogenesis-receptor activation, EGFR tyrosine kinase inhibitor resistance, Endocrine resistance, ErbB signaling pathway, Human cytomegalovirus infection, Non-small cell lung cancer, Pancreatic cancer and PI3K-Akt signaling pathway (**Figure 2E**).

The classification of molecular subtypes in SKCM through 70 DE-ARGs

To identify the molecular subtypes of SKCM, we performed an unsupervised consensus clustering analysis of 471 SKCM samples from TCGA-SKCM database based on the expressions of the 70 DE-ARGs (**Figure 3A** and **3B**). By setting the K value in the range of 2-6 and choosing the optimal K = 2, two molecular subtypes of SKCM were identified, among which, group 1 and group 2 respectively contained 420 and 51 samples (**Figure 3C**). Subsequently, the DEGs in the two molecular subtypes of SKCM were identified, and the corresponding volcano plot and heatmap of these DEGs were presented in **Figure 3D** and **3E**, respectively. GO analysis proved that the DEGs were mainly relevant with DNA and RNA localization and replication, metabolic progress, biosynthetic progress (**Figure 3F** and **3G**). Furthermore, the KEGG analysis revealed that the DEGs were mainly enriched in metabolism, kinds of signaling pathways, and cancers (**Figure 3H** and **3I**).

Comparison between the two molecular subtypes of SKCM

We next attempted to investigate the difference of clinical information, ferroptosis-related genes, m6A-related genes, immune checkpoints and overall survivals between the two molecular subtypes of SKCM. Among these clinical information, there were significant difference between the two molecular subtypes of SKCM in pTMN stage and radiotherapy (**Figure 4A** and **4B**). Additionally, all the ferroptosis-related genes were highly expressed in group 1 which included 420 SKCM samples when compared with group 2 (**Figure 4C**). Similar results were also obtained from m6A-related genes that all these genes were up-regulated in group 1 than that in group 2 (**Figure 4D**). Then, the expression of immune checkpoints, including CTLA4, CD274, PDCD1LG2, HAVCR2 and TIGIT in group 1, was notably up-regulated than that in group 2 (**Figure 4E**). The overall survival analysis suggested that the group 2 had better prognosis than that of group 1 (**Figure 4F**).

Survival analysis of the 70 DE-ARGs

Next, we utilized univariate cox regression analysis to determine which words to employ in building the nomogram, and we used the "forestplot" R package to display the *P* values, HRs, and 95% CIs for each of the 70 DE-ARGs. The "forestplot" package in R is a package used to create forest plots, which are often used in meta-analyses to display the effect sizes of individual studies along with a summary effect size. These plots are a popular way of visualizing the results from a systematic review or meta-analysis, showing both the individual study estimates and the combined meta-analysis estimate. According to the data, among the 70 DE-ARGs, there were 18 genes (18 DE-ARGs), including APOL1, CAPNS1, CCR2,

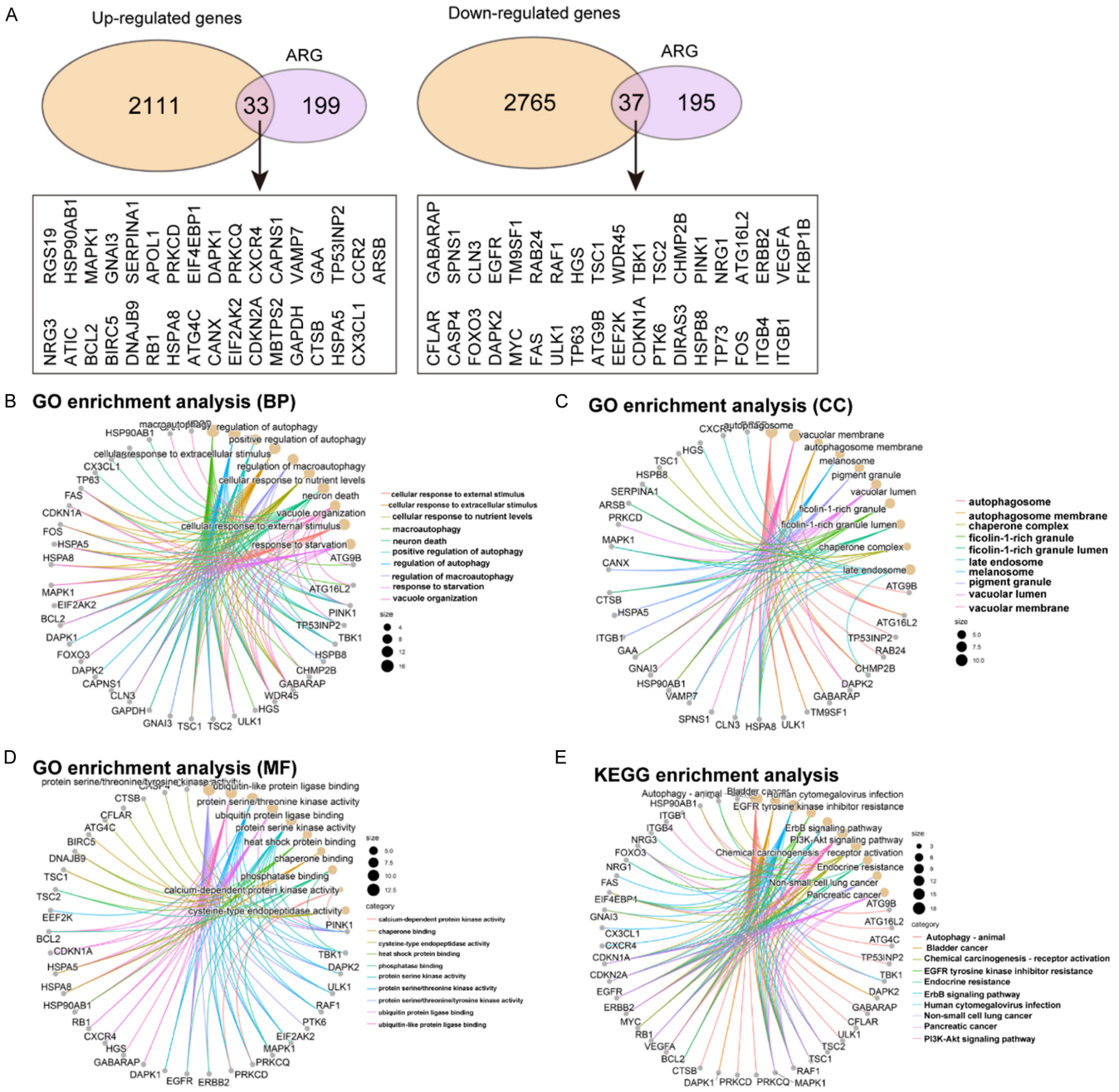
A
Up-regulated genes
ARG
2111
33
199
RGS19
HSP90AB1
MAPK1
GNAI3
SERPINA1
APOL1
PRKCD
EIF4EBP1
DAPK1
PRKCQ
CXCR4
CAPNS1
VAMP7
GAA
TP53INP2
CCR2
ARSB
NRG3
ATIC
BCL2
BIRC5
DNAJB9
RB1
HSPA8
ATG4C
CANX
EIF2AK2
CDKN2A
MBTPS2
GAPDH
CTSB
HSPA5
CX3CL1
Down-regulated genes
ARG
2765
37
195
GABARAP
SPNS1
CLN3
EGFR
TM9SF1
RAB24
RAF1
HGS
TSC1
WDR45
TBK1
TSC2
CHMP2B
PINK1
NRG1
ATG16L2
ERBB2
VEGFA
FKBP1B
CFLAR
CASP4
FOXO3
DAPK2
MYC
FAS
ULK1
TP63
ATG9B
EEF2K
CDKN1A
PTK6
DIRAS3
HSPB8
TP73
FOS
ITGB4
ITGB1
B
GO enrichment analysis (BP)
macroautophagy
regulation of autophagy
positive regulation of autophagy
cellular response to extracellular stimulus
regulation of macroautophagy
cellular response to nutrient levels
neuron death
vacuole organization
cellular response to external stimulus
response to starvation
cellular response to external stimulus
cellular response to extracellular stimulus
cellular response to nutrient levels
macroautophagy
neuron death
positive regulation of autophagy
regulation of autophagy
regulation of macroautophagy
response to starvation
vacuole organization
size
C
GO enrichment analysis (CC)
autophagosome
vacuolar membrane
autophagosome membrane
melanosome
pigment granule
vacuolar lumen
ficolin-1-rich granule
ficolin-1-rich granule lumen
chaperone complex
late endosome
autophagosome
autophagosome membrane
chaperone complex
ficolin-1-rich granule
ficolin-1-rich granule lumen
late endosome
melanosome
pigment granule
vacuolar lumen
vacuolar membrane
size
D
GO enrichment analysis (MF)
ubiquitin-like protein ligase binding
protein serine/threonine kinase activity
ubiquitin protein ligase binding
protein serine kinase activity
heat shock protein binding
chaperone binding
phosphatase binding
calcium-dependent protein kinase activity
cysteine-type endopeptidase activity
size
category
calcium-dependent protein kinase activity
chaperone binding
cysteine-type endopeptidase activity
heat shock protein binding
phosphatase binding
protein serine kinase activity
protein serine/threonine kinase activity
protein serine/threonine/tyrosine kinase activity
ubiquitin protein ligase binding
ubiquitin-like protein ligase binding
E
KEGG enrichment analysis
Autophagy - animal
Bladder cancer
Human cytomegalovirus infection
EGFR tyrosine kinase inhibitor resistance
ErbB signaling pathway
PI3K-Akt signaling pathway
Chemical carcinogenesis - receptor activation
Endocrine resistance
Non-small cell lung cancer
Pancreatic cancer
size
category
Autophagy - animal
Bladder cancer
Chemical carcinogenesis - receptor activation
EGFR tyrosine kinase inhibitor resistance
Endocrine resistance
ErbB signaling pathway
Human cytomegalovirus infection
Non-small cell lung cancer
Pancreatic cancer
PI3K-Akt signaling pathway

Figure 2. Overlap genes obtainment and functional analysis. A. Overlap genes between up- or down-regulated genes in SKCM and 232 autophagy-related genes (ARGs). The 70 overlap genes were named as DE-ARGs in the present study. B. BP of GO analysis. C. CC of GO analysis. D. Molecular function (MF) of GO analysis. E. KEGG analysis of the overlap genes.

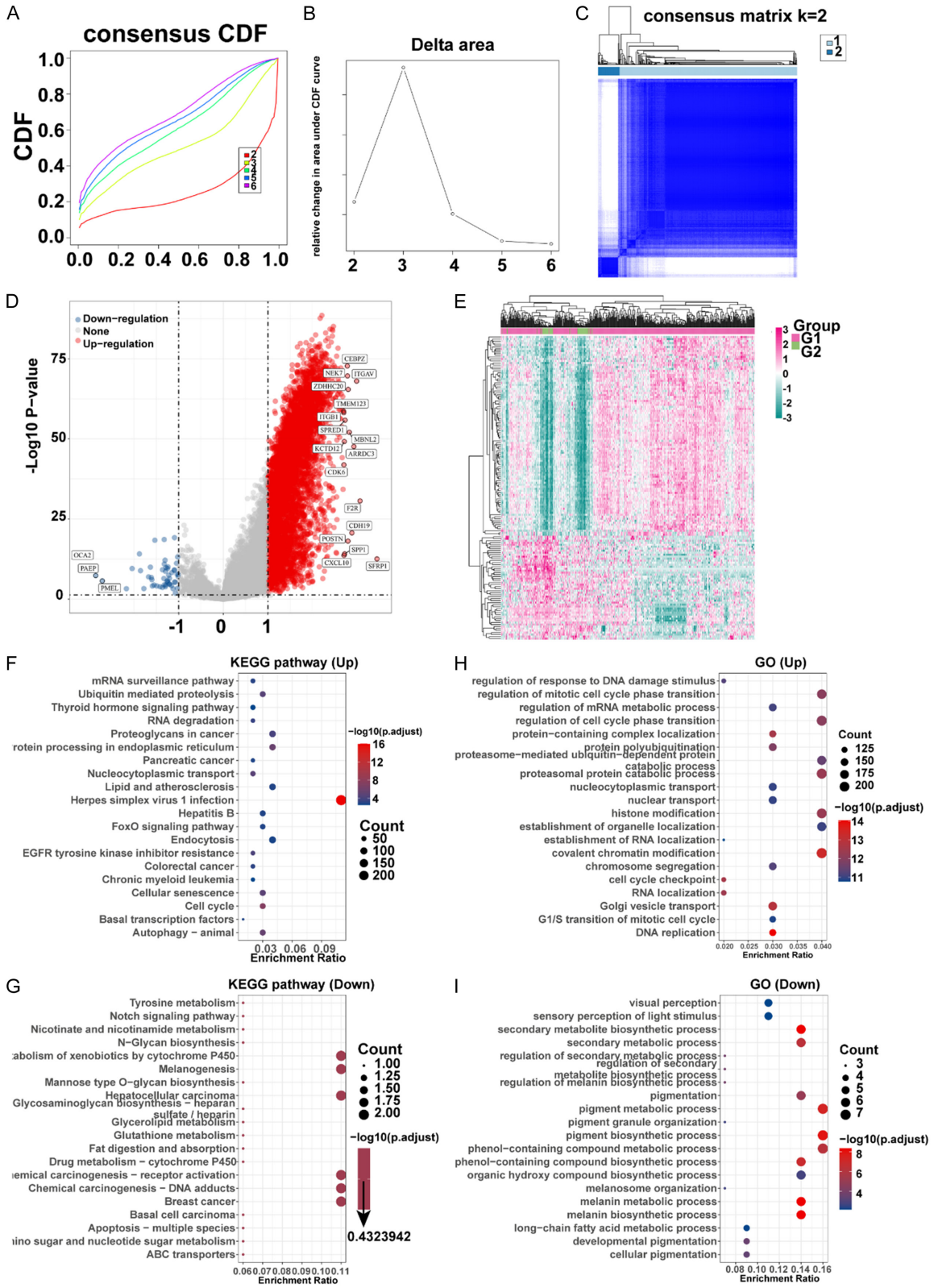

Figure 3. Molecular subtypes identification in SKCM. A. The cumulative distribution function (CDF) curves (k = 2, 3, 4, 5, and 6) in consensus cluster analysis. B. Relative change in area under the CDF curve when k = 2-6. C. The heatmap related to the consensus matrix for k = 2. D, E. Deferentially expressed genes (DEGs) analysis of the two molecular subtypes in SKCM. The volcano plot and heatmap were respectively shown. Group 1: 420 SKCM samples; Group 2: 51 SKCM samples. F, G. GO analysis of the up- or down-DEGs of the two molecular subtypes in SKCM. H, I. KEGG analysis of the up- or down-DEGs of the two molecular subtypes in SKCM.

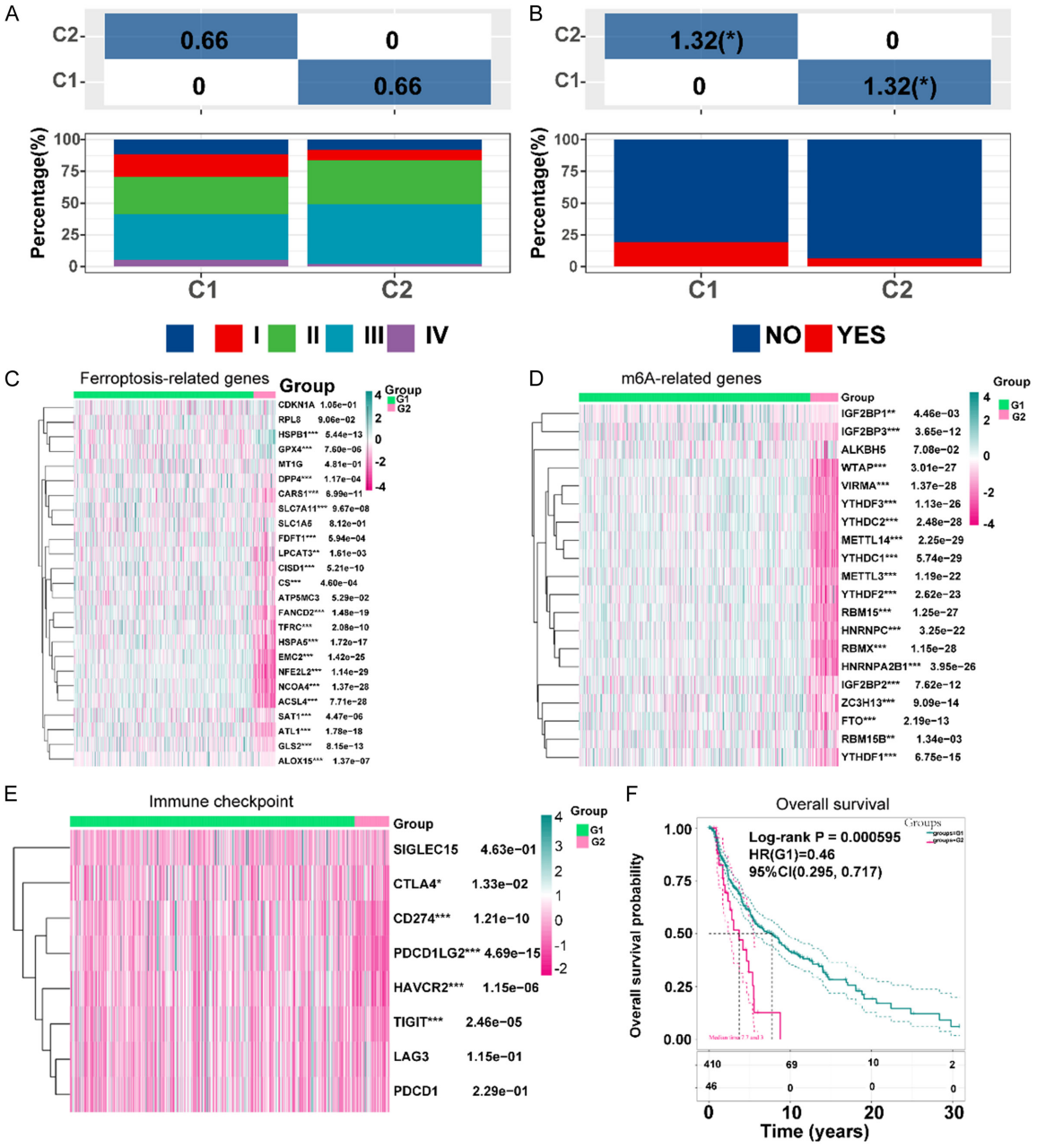

Figure 4. Comparison of the clinical information, ferroptosis-related genes, m6A-related genes, immune checkpoints and overall survival between the two molecular subtypes in SKCM. A. pTMN stage difference in the two molecular subtypes. B. Radiotherapy comparison. C. The expression of ferroptosis-related genes in the two molecular subtypes. D. The expression of m6A-related genes in the two molecular subtypes. E. The expression of immune checkpoints in the two molecular subtypes. F. Overall survival analysis between the two molecular subtypes. *p-value < 0.05, **p-value < 0.01, ***p-value < 0.001.

CXCR4, EIF4EBP1, PRKCQ, RGS19, SERPINA1, BIRC5, DNAJB9, EGFR, CASP4, CFLAR, ATG9B, DAPK2, FAS, PTK6 and ULK1, which had a *P* value less than 0.05 (**Figure 5A**). Besides, the overall survival analysis of these 18 genes was also evaluated by GEPIA database, and higher expression of most of these 18 genes except ATG9B, BIRC5, CAPNS1, EIF4EBP1, EGFR, PTK6 and ULK1, had better prognosis (**Figure 5B**).

Gene correlation analysis of 18 DE-ARGs in SKCM and PPI network construction

Next, we sought to assess the expression correlation of the above obtained 18 DE-ARGs in 471 SKCM samples. A heatmap of the correlation between the 18 DE-ARGs was generated and the data suggested that PTK6, ATG9B, ULK1, CAPNS1, BIRC5, CAPNS1 and EIF4EBP1 was negatively correlated with most of the 18 DE-ARGs in SKCM (Figure S1A). Moreover, the protein-protein interacting (PPI) network of these 18 DE-ARGs was generated by using STRING database, and the results revealed that BIRC5, EGFR, CFLAR, CXCR4, CCR2 and FAS were placed in the interacting center of the PPI network (Figure S1B).

Expression and survival analysis of the 18 DE-ARGs in pan-cancers

The expression of the 18 DE-ARGs in pan-cancers was then evaluated by using GSCA database based on TCGA data, and the results from the bubble plot demonstrated that most of the 18 DE-ARGs exhibited high expression in KIRC, KIRP, THCA and BRCA (Figure S2A). Additionally, the 18 DE-ARGs expression in pathologic stages of pan-cancers was also studied, and the heatmap indicated that a half of 18 DE-ARGs expression was higher in most cancers' stage III and IV (Figure S2B). The subtype difference of pan-cancers between high and low gene expression of the 18 DE-ARGs was also assessed and the results certified that significant difference between high and low gene expression of the 18 DE-ARGs were observed in BRCA, KIRC, GBM, LUAD, LUSC and STAD (Figure S2C). Finally, the survivals including OS, PFS, DSS and DFI, were analyzed, and the data suggested that most of the 18 DE-ARGs' higher expression was positively correlated with good OS, PFS and DSS in KIRC, LGG, PAAD, and LUSC (Figure S2D).

Genetic changes analysis of the 18 DE-ARGs in pan-cancers

Next, the genetic alteration including SNV and CNV of the 18 DE-ARGs in pan-cancers were analyzed. The SNV percentage heatmap indicated that a number of the 18 DE-ARGs had high mutation frequency in UCEC, SKCM, COAD, GBM, LUAD, LUSC and STAD (Figure S3A). Then, waterfall plot suggested that the top 10 mutated genes in pan-cancers were EGFR, PRKCQ, ULK1, ATG9B, CCR2, SERPINA1, CASP4, FAS, CXCR4, and DAPK2 (Figure S3B). Furthermore, the CNV landscape including heterozygous amplification, homozygous amplification, heterozygous deletion, homozygous deletion, in pan-cancers was also evaluated. The bubble plots indicated that most of the 18 DE-ARGs had heterozygous amplification and heterozygous deletion in most cancer types (Figure S3C and S3D). Subsequently, the correlation of CNV and the 18 DE-ARGs expression in TCGA cancer types were analyzed, and the results from the bubble plot suggested that the most of the 18 DE-ARGs' expression was positively correlated with their corresponding CNV in LUSC, BRCA, OV, HNSC, LUAD, BLCA and LIHC (Figure S3E).

Methylation analysis of the 18 DE-ARGs in pan-cancers and SKCM

A plethora of studies had suggested that gene methylation served as critical roles in cancer development and progression. We thereby next studied the methylation of the 18 DE-ARGs in pan-cancers and SKCM. The methylation difference in each cancer was investigated and the bubble plot suggested that the majority of the18 DE-ARGs exhibited methylation difference between tumor samples and normal tissues in KIRC, LUSC, LIHC, KIRP, and UCEC (Figure S4A). Moreover, the correlation between the 18 DE-ARGs' methylation and their corresponding mRNA expression was also assessed and the results certified that most of 18 DE-ARGs DNA methylation was negatively related with their corresponding mRNA expression in pan-cancers (Figure S4B). Additionally, the analysis of survival difference including OS, PFS, DSS and DFI between high and low methylation was analyzed, and the data suggested that the most 18 DE-ARGs' methylation had no significant affection on survivals in most TCGA cancer types (Figure S4C). The correlation of

A

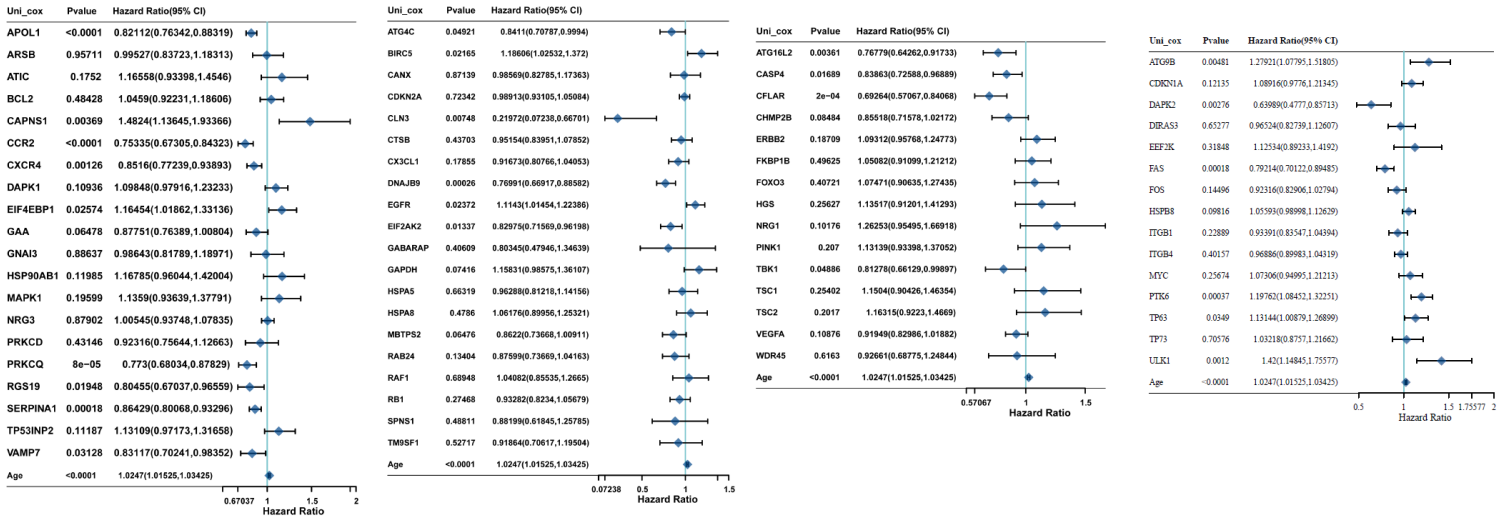
Uni_cox Pvalue Hazard Ratio(95% CI)
APOL1 <0.0001 0.82112(0.76342,0.88319)
ARSB 0.95711 0.99527(0.83723,1.18313)
ATIC 0.1752 1.16558(0.93398,1.4546)
BCL2 0.48428 1.0459(0.92231,1.18606)
CAPNS1 0.00369 1.4824(1.13645,1.93366)
CCR2 <0.0001 0.75335(0.67305,0.84323)
CXCR4 0.00126 0.8516(0.77239,0.93893)
DAPK1 0.10936 1.09848(0.97916,1.23233)
EIF4EBP1 0.02574 1.16454(1.01862,1.33136)
GAA 0.06478 0.87751(0.76389,1.00804)
GNAI3 0.88637 0.98643(0.81789,1.18971)
HSP90AB1 0.11985 1.16785(0.96044,1.42004)
MAPK1 0.19599 1.1359(0.93639,1.37791)
NRG3 0.87902 1.00545(0.93748,1.07835)
PRKCD 0.43146 0.92316(0.75644,1.12663)
PRKCQ 8e−05 0.773(0.68034,0.87829)
RGS19 0.01948 0.80455(0.67037,0.96559)
SERPINA1 0.00018 0.86429(0.80068,0.93296)
TP53INP2 0.11187 1.13109(0.97173,1.31658)
VAMP7 0.03128 0.83117(0.70241,0.98352)
Age <0.0001 1.0247(1.01525,1.03425)
0.67037 1 1.5 2
Hazard Ratio
Uni_cox Pvalue Hazard Ratio(95% CI)
ATG4C 0.04921 0.8411(0.70787,0.9994)
BIRC5 0.02165 1.18606(1.02532,1.372)
CANX 0.87139 0.98569(0.82785,1.17363)
CDKN2A 0.72342 0.98913(0.93105,1.05084)
CLN3 0.00748 0.21972(0.07238,0.66701)
CTSB 0.43703 0.95154(0.83951,1.07852)
CX3CL1 0.17855 0.91673(0.80766,1.04053)
DNAJB9 0.00026 0.76991(0.66917,0.88582)
EGFR 0.02372 1.1143(1.01454,1.22386)
EIF2AK2 0.01337 0.82975(0.71569,0.96198)
GABARAP 0.40609 0.80345(0.47946,1.34639)
GAPDH 0.07416 1.15831(0.98575,1.36107)
HSPA5 0.66319 0.96288(0.81218,1.14156)
HSPA8 0.4786 1.06176(0.89956,1.25321)
MBTPS2 0.06476 0.8622(0.73668,1.00911)
RAB24 0.13404 0.87599(0.73669,1.04163)
RAF1 0.68948 1.04082(0.85535,1.2665)
RB1 0.27468 0.93282(0.8234,1.05679)
SPNS1 0.48811 0.88199(0.61845,1.25785)
TM9SF1 0.52717 0.91864(0.70617,1.19504)
Age <0.0001 1.0247(1.01525,1.03425)
0.07238 0.5 1 1.5
Hazard Ratio
Uni_cox Pvalue Hazard Ratio(95% CI)
ATG16L2 0.00361 0.76779(0.64262,0.91733)
CASP4 0.01689 0.83863(0.72588,0.96889)
CFLAR 2e−04 0.69264(0.57067,0.84068)
CHMP2B 0.08484 0.85518(0.71578,1.02172)
ERBB2 0.18709 1.09312(0.95768,1.24773)
FKBP1B 0.49625 1.05082(0.91099,1.21212)
FOXO3 0.40721 1.07471(0.90635,1.27435)
HGS 0.25627 1.13517(0.91201,1.41293)
NRG1 0.10176 1.26253(0.95495,1.66918)
PINK1 0.207 1.13139(0.93398,1.37052)
TBK1 0.04886 0.81278(0.66129,0.99897)
TSC1 0.25402 1.1504(0.90426,1.46354)
TSC2 0.2017 1.16315(0.9223,1.4669)
VEGFA 0.10876 0.91949(0.82986,1.01882)
WDR45 0.6163 0.92661(0.68775,1.24844)
Age <0.0001 1.0247(1.01525,1.03425)
0.57067 1 1.5
Hazard Ratio
Uni_cox Pvalue Hazard Ratio(95% CI)
ATG9B 0.00481 1.27921(1.07795,1.51805)
CDKN1A 0.12135 1.08916(0.9776,1.21345)
DAPK2 0.00276 0.63989(0.4777,0.85713)
DIRAS3 0.65277 0.96524(0.82739,1.12607)
EEF2K 0.31848 1.12534(0.89233,1.4192)
FAS 0.00018 0.79214(0.70122,0.89485)
FOS 0.14496 0.92316(0.82906,1.02794)
HSPB8 0.09816 1.05593(0.98998,1.12629)
ITGB1 0.22889 0.93391(0.83547,1.04394)
ITGB4 0.40157 0.96886(0.89983,1.04319)
MYC 0.25674 1.07306(0.94995,1.21213)
PTK6 0.00037 1.19762(1.08452,1.32251)
TP63 0.0349 1.13144(1.00879,1.26899)
TP73 0.70576 1.03218(0.8757,1.21662)
ULK1 0.0012 1.42(1.14845,1.75577)
Age <0.0001 1.0247(1.01525,1.03425)
0.5 1 1.5 1.75577 2
Hazard Ratio

B

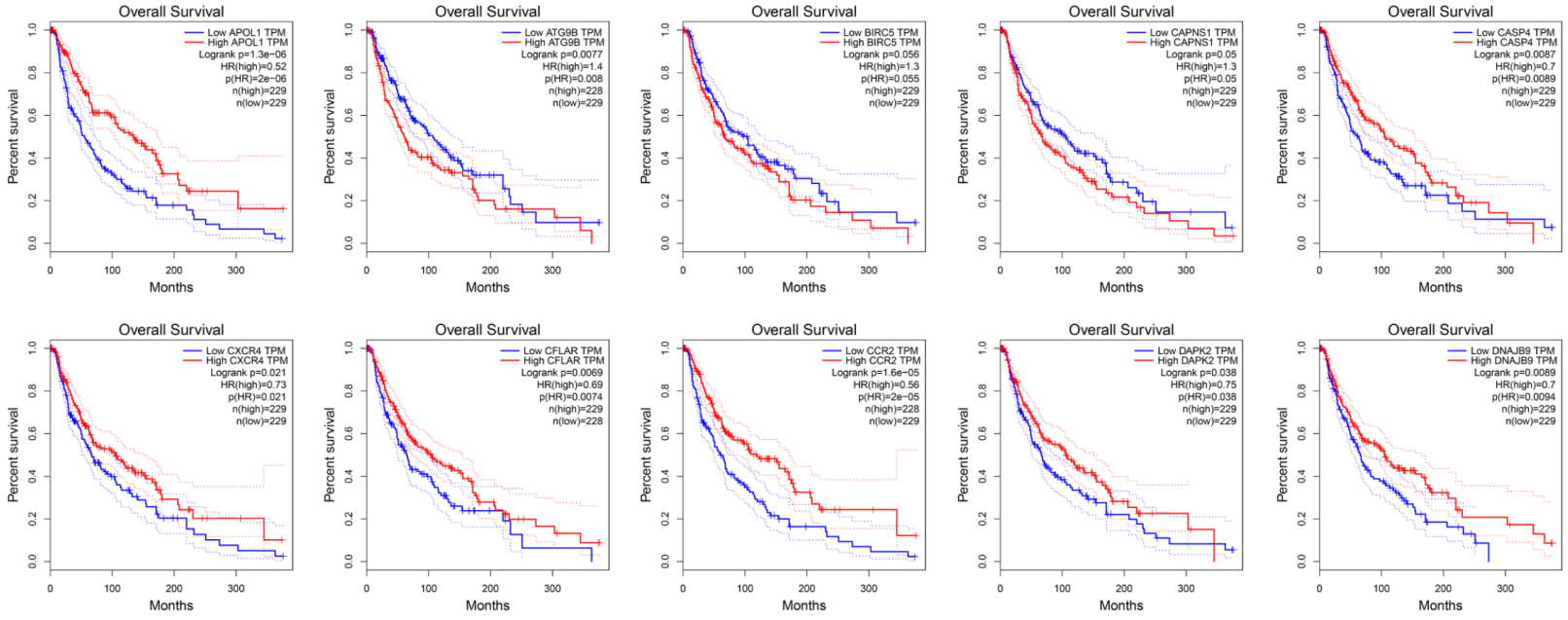
Overall Survival
Low APOL1 TPM
High APOL1 TPM
Logrank p=1.3e−06
HR(high)=0.52
p(HR)=2e−06
n(high)=229
n(low)=229
Overall Survival
Low ATG9B TPM
High ATG9B TPM
Logrank p=0.0077
HR(high)=1.4
p(HR)=0.008
n(high)=228
n(low)=229
Overall Survival
Low BIRC5 TPM
High BIRC5 TPM
Logrank p=0.056
HR(high)=1.3
p(HR)=0.055
n(high)=229
n(low)=229
Overall Survival
Low CAPNS1 TPM
High CAPNS1 TPM
Logrank p=0.05
HR(high)=1.3
p(HR)=0.05
n(high)=229
n(low)=229
Overall Survival
Low CASP4 TPM
High CASP4 TPM
Logrank p=0.0087
HR(high)=0.7
p(HR)=0.0089
n(high)=229
n(low)=229
Overall Survival
Low CXCR4 TPM
High CXCR4 TPM
Logrank p=0.021
HR(high)=0.73
p(HR)=0.021
n(high)=229
n(low)=229
Overall Survival
Low CFLAR TPM
High CFLAR TPM
Logrank p=0.0069
HR(high)=0.69
p(HR)=0.0074
n(high)=229
n(low)=228
Overall Survival
Low CCR2 TPM
High CCR2 TPM
Logrank p=1.6e−05
HR(high)=0.56
p(HR)=2e−05
n(high)=228
n(low)=229
Overall Survival
Low DAPK2 TPM
High DAPK2 TPM
Logrank p=0.038
HR(high)=0.75
p(HR)=0.038
n(high)=229
n(low)=229
Overall Survival
Low DNAJB9 TPM
High DNAJB9 TPM
Logrank p=0.0089
HR(high)=0.7
p(HR)=0.0094
n(high)=229
n(low)=229
Percent survival
Months

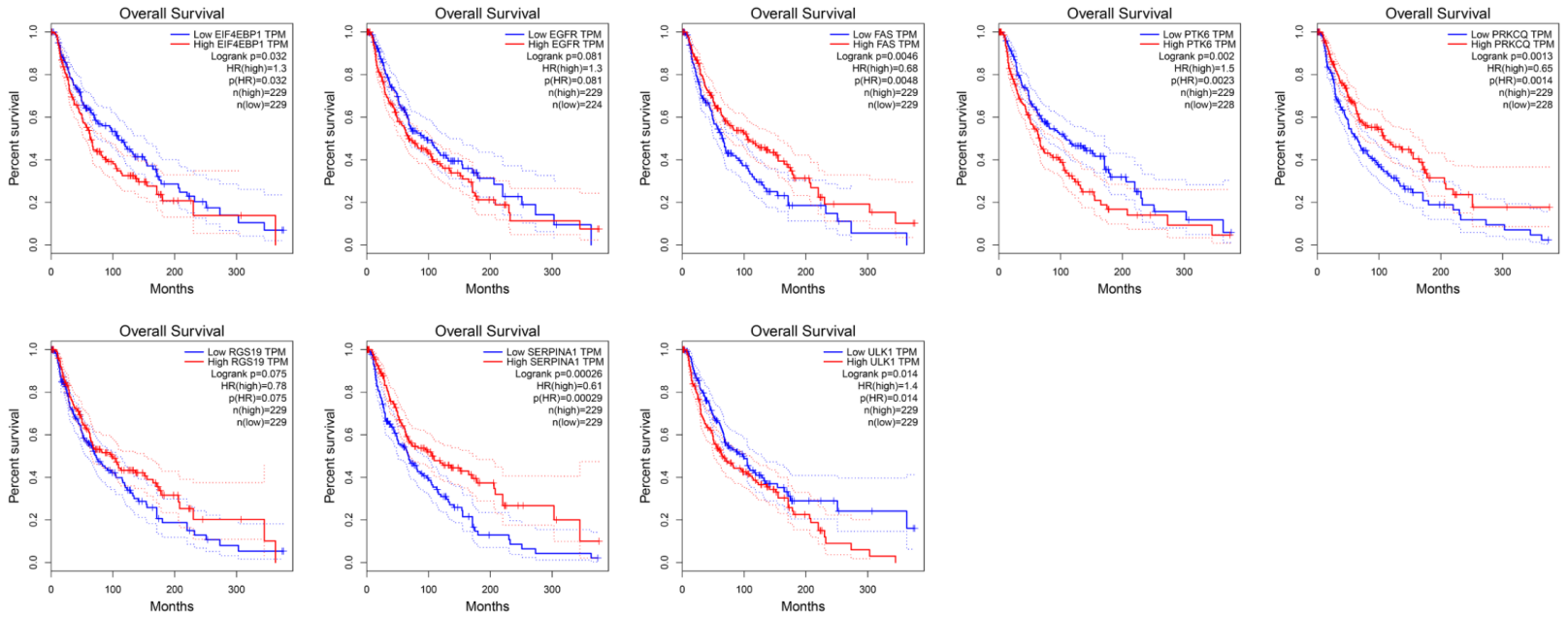

Figure 5. Univariate cox regression analysis and overall survival analysis of DE-ARGs in SKCM. A. Univariate cox regression analysis. B. GEPIA database was utilized for analyzing the overall survivals of the DE-ARGs, and there were 18 DE-ARGs with significant difference.

the 18 DE-ARGs methylation and their corresponding mRNA expression in SKCM was also investigated, and the results demonstrated that nearly all the 18 DE-ARGs' methylation was negatively correlated with their corresponding expression in SKCM (Figure S4D).

Genetic changes and methylation of the 18 DE-ARGs in SKCM

The expression difference of the 18 DE-ARGs between pathologic stages in SKCM was then investigated, and the results suggested that CCR2, CFLAR, CXCR4, DNAJB9 and PRKCQ had remarkable expression difference between pathologic stages in SKCM (Figure S5A). Afterwards, the SNV analysis from the waterfall plot indicated that the top 10 mutated genes were DAPK2, PTK6, FAS, SERPINA1, ATG9B, APOL1, CCR2, ULK1, EGFR and PRKCQ (Figure S5B). The CNV analysis from the pie plot demonstrated that most of the 18 DE-ARGs had heterozygous amplification and heterozygous deletion in SKCM (Figure S5C). The correlations between CNV and mRNA expression of all the 18 DE-ARGs were positive (Figure S5D). The survival difference including OS, PFS and DSS, between CNV groups was also evaluated, and the data suggested that nearly all the 18 DE-ARGs had no significant difference between the CNV groups in SKCM (Figure S5E). Then, the correlation between methylation and 18 DE-ARGs mRNA expression was also explored, and the data proved that all the 18 DE-ARGs mRNA expression was positively correlated with low methylation (Figure S5F). The analysis of the survival difference including OS, PFS and DSS, between high and low methylation in each cancer revealed that there were obvious survival difference between FAS, CXCR4, RGS19, CFLAR and APOL1 high and low methylation in SKCM (Figure S5G).

Immune interacting network of 18 DE-ARGs in SKCM

Numerous reports had uncovered that many genes had effect on cancer development and progression via regulating immune cells. We thus sought to construct the immune interacting network of 18 DE-ARGs in SKCM. By using R software "immuneeconv" package, the heatmaps of 18 DE-ARGs' immune interacting network were generated based on EPIC and CIBERSORT algorithms, respectively. The data suggested that the 18 DE-ARGs were dramatically related with kinds of immune cells such as NK cell, Macrophage, Endothelial cell, T cells, B cell (Figure S6A and S6B).

Construction of the autophagy-related genes prognostic signature

The above analyses had revealed that the 18 DE-ARGs were closely relevant with SKCM survivals, we thus carried out the LASSO regression to construct the prognostic signature in SKCM. The coefficient of 18 DE-ARGs was presented in Figure S7A. The model was able to obtain the best fit when 12 of the 18 DE-ARGs were included (Figure S7B). The formula used for risk score computation was as follows: Riskscore = (-0.0932)*APOL1 + (0.0838)*CAPNS1 + (-0.1644)*RGS19 + (0.1146)*BIRC5 + (-0.123)*DNAJB9 + (0.1065)*EGFR + (-0.0933)*CFLAR + (0.0499)*ATG9B + (-0.2451)*DAPK2 + (-0.0515)*FAS + (0.1117)*PTK6 + (0.2023)*ULK1. The risk score model used a median threshold to classify 471 SKCM tumor samples into low- or high-risk subgroups, and a heatmap of the 12 genes (12 DE-ARGs) in SKCM was also created (Figure S7C). Besides, the overall survival analysis presented that the high-risk group had notably poor overall survivals (Figure S7D). Receiver operating characteristic (ROC) analysis that takes into account the passage of time was also used to evaluate the prognostic model's performance. One-year, three-year, and five-year overall survival (OS) area under the ROC curve (AUC) values were 0.724, 0.696, and 0.711, respectively (Figure S7E).

The correlation between the autophagy-related genes prognostic signature and immune cells

To investigate the association between our ARGs prognostic signature and immune infiltration cell types, the correlations between the above obtained ARGs prognostic signature and immune score was analyzed with the R software "ggstatsplot" package. According to the results, our ARGs prognostic signature was remarkably negatively correlated with B cell, CD8+ T cell, CD4+ T cell, Macrophage, Neutrophil and Myeloid dendritic cell in SKCM (Figure S8A-F).

GSVA analysis of the 12 DE-ARGs

Given that our above analyses constructed 12 DE-ARGs prognostic signature in SKCM, we

next attempted to use the 12 genes (APOL1, CAPNS1, RGS19, BIRC5, DNAJB9, EGFR, CFLAR, ATG9B, DAPK2, FAS, PTK6, ULK1) as a whole gene list to evaluate the Gene Set Variation Analysis (GSVA) score by using R software package "GSVA". The GSVA score is positively correlated with the expression of the 12 DE-ARGs list, and we found that the 12 DE-ARGs list had high GSVA score in tumor samples than that of the normal tissues in BLCA, ESCA, HNSC, KICH, KIRC, KIRP, and THCA (Figure S9A). Moreover, the GSVA score in stages (stage I, II, III and IV) of TCGA cancer types was further evaluated (Figure S9B). Additionally, the relationship between kinds of signaling pathway activity and the GSVA score was also assessed, and the results demonstrated that the 12 DE-ARGs list was notably positively correlated with TSC/mTOR, RTK, RAS/MAPK, EMT and apoptosis in most cancer types, while negatively relevant with cell cycle, DNA damage, Hormone AR (Figure S9C). Finally, the survival analysis of the high and low GSVA score revealed that higher GSVA score had poor OS, PFS, and DSS in KIRC, KIRP, LGG, LUAD, PAAD, THYM and UVM (Figure S9D).

CAPNS1 expression and methylation analysis in pan-cancers

Since our above analysis indicated that the 12 DE-ARGs might play crucial roles in cancers, we next wonder whether there was a potential target gene in the 12 DE-ARGs which had important roles in in regulating SKCM development and progression. Among the 12 DE-ARGs, we selected CAPNS1 for further study because that there is still few studies about CAPNS1 functions in cancers especially in SKCM and many other genes have been reported in many tumors, including SKCM. We first evaluated CAPNS1 expression in kinds of normal tissues and cells by using Harmonizome 3.0 database, and it was found that CAPNS1 expressed widely in numerous normal tissues and cells (Figure S10A). Subsequently, the CAPNS1 expression levels in pan-cancers were then assessed using TIMER database, and we found that most tumor tissues expressed CAPNS1, and it was high expression in many cancers such as UCEC, THCA, STAD, PCPG, PAAD, LIHC, KIRP, ESCA and BLCA (Figure S10B). Besides, the protein levels of CAPNS1 in kinds of cancer types were also evaluated via using HPA database (Figure S10C). Finally, the CAPNS1 methylation levels across TCGA cancer types were further investigated by using GSCA database (Figure S10D).

Immune cell infiltration, immune checkpoints, TMB and MSI analyses of CAPNS1 in pan-cancers

Immune cell infiltration was critical in melanoma tumorigenesis and metastasis. Therefore, we next attempted to evaluate the correlation between CAPNS1 expression and multiple immune cell infiltration in pan-cancers using different immune score algorithms such as EPIC, CIBERSORT, XCELL, QUANTSEQ. By using TIMER database, the results were obtained and displayed with heatmap (Figure S11). The data suggested that there was positive correlation between CAPNS1 expression and NK cell, Myeloid dendritic cell, Macrophage, and monocyte in most cancer types. In addition, the relationships between CAPNS1 expressions and the immune checkpoints (TIGIT, SIGLEC15, PDCD1LG2, PDCD1, LAG3, HAVCR2, CTLA4 and CD274) was also assessed, and the data suggested that CAPNS1 expression was positively correlated with the immune checkpoints in half of the TCGA cancers such as ACC, BLCA, CESC, HNSC, KICH, LGG, LIHC, MESO, OV, PCPG, SARC, and STAD (Figure S12A). Afterwards, the correlation of CAPNS1 and TMB (tumor mutation burden) and MSI (microsatellite instability) across cancer types was determined. According to the dot plots, the CAPNS1 was positively correlated with TMB and MSI in half of the pan-cancers, while negatively related with TMB and MSI in the rest of the TCGA cancers (Figure S12B and S12C).

CAPNS1 is a prognostic factor in SKCM

Firstly, the CAPNS1 expression in SKCM tumor samples was assessed by using GEPIA database. Since the TCGA-SKCM data had no control normal tissues of SKCM, we used GTEx data as control, and the dot plot showed that CAPNS1 expression was higher in SKCM samples (Figure S13A). In addition, the immunohistochemistry analyses from HPA database also suggested that CAPNS1 was high expression in melanoma tumor tissues than that in normal skin tissues (Figure S13B). Afterwards, the CAPNS1 expression from low level to high level, the CAPNS1 expression distribution in SKCM tissue samples with live or dead, and the

expression heatmap of CAPNS1 was also analyzed (Figure S13C). High CAPNS1 expression was associated with a poor prognosis in SKCM, as shown by an overall survival analysis of 471 SKCM samples that were separated into high and low CAPNS1 expression groups (Figure S13D). The ROC curve of CAPNS1 in SKCM was also analyzed, and the results showed that 3-year, 4-year and 5-year AUC value was 0.585, 0.58 and 0.597, respectively, which suggested that CAPNS1 might be a prognostic signature for SKCM (Figure S13E).

The immune correlation between CAPNS1 and immune cells and immune interacting network construction

We next wonder whether CAPNS1 was correlated with immune cells. To achieve that, we first applied GSCA database to analyze the correlation between CAPNS1 and multiple immune cells. As the data presented in Figure S14A, CAPNS1 was positively correlated with NK, γδT cell, macrophage, DC, infiltration score, while negatively related with nTreg, central memory infiltration, iTreg, CD4 naive infiltration. Moreover, the immune interacting network between CAPNS1 and kinds of immune cells was generated by using R software "immuneeconv" package based on CIBERSORT algorithm, and the data certified that CAPNS1 was remarkably related with kinds of immune cells (Figure S14B).

Construction of CAPNS1 interacting network and molecular subtypes in SKCM identification

The interacting network of CAPNS1 was then investigated by using Genemania database. According to the interacting network, CAPNS1 was able to interact with CAPN1, CAST, CAPN2, ALDH7A1, CAPNS2, HTT, ECH1, C8orf37, FLG, PPP2R1A, BCAP31, ACTN4, CDH1, GNB2, CSPG4, RNH1, RUVBL1, ARHGDIA, TUBGCP2, and IGFBP6 (Figure S15A). Subsequently, we wonder whether these CAPNS1-related genes was capable to identify novel molecular subtypes of SKCM. To achieve that, an unsupervised consensus clustering analysis of 471 SKCM samples from TCGA-SKCM database based on the expressions of the above 20 CAPNS1-related genes (Figure S15B and S15C). By setting the K value in the range of 2-6 and choosing the optimal K = 3, three molecular subtypes of SKCM were clarified, among which, group 1 (C1), group 2 (C2) and group 3 (C3) respectively contained 362, 65 and 44 SKCM samples (Figure S15D). The DEGs in the three molecular subtypes of SKCM were identified, and the corresponding heatmap was presented in Figure S15E.

Immune checkpoints and cells analysis in the three molecular subtypes in SKCM

Firstly, the overall survivals of the above obtained novel three molecular subtypes in SKCM were analyzed, and group 3 showed the lowest overall survival when compared with group 1 and group 2 (**Figure 6A**). Thereafter, the expression of immune checkpoints in the three molecular subtypes in SKCM was further studied, and the results suggested that most of the immune checkpoints exhibited significant expression difference in the three molecular subtypes of SKCM (**Figure 6B**). Finally, the CIBERSORT algorithm was used to evaluate the immune scores of multiple immune cells in three molecular subtypes of SKCM. The data suggested that there was significant difference of B cell naive, B cell memory, B cell plasma, T cell CD8+, T cell CD4+ memory resting, T cell CD4+ memory activated, T cell gamma delta, NK cell resting, NK cell activated, Macrophage M2, Myeloid dendritic cell resting, Myeloid dendritic cell activated, Mast cell activated, and Neutrophil (**Figure 6C**, **6D**).

CAPNS1 knockdown suppressed melanoma cells growth

Considering our above studies proved that CAPNS1 was closely correlated with SKCM, we next attempted to investigate its functions using experiments. Firstly, we used CCLE database to uncover the CAPNS1 expression levels in 54 melanoma cell lines, and we found that CAPNS1 was highly expressed in all the melanoma cell lines (**Figure 7A**). Subsequently, we performed qRT-PCR assays to examine the CAPNS1 expression levels in several melanoma cell lines including SK-MEL-24, A-375, SK-MEL-1, SK-MEL-28, A2058, and a control cell line HEMa-LP. The data suggested that these cell lines highly expressed CAPNS1, and A-375 and SK-MEL-28 expressed the highest CAPNS1 among these cells (**Figure 7B**). Therefore, we next chose A-375 and SK-MEL-28 cells for experiments. The qRT-PCR assays were also applied for the determination of

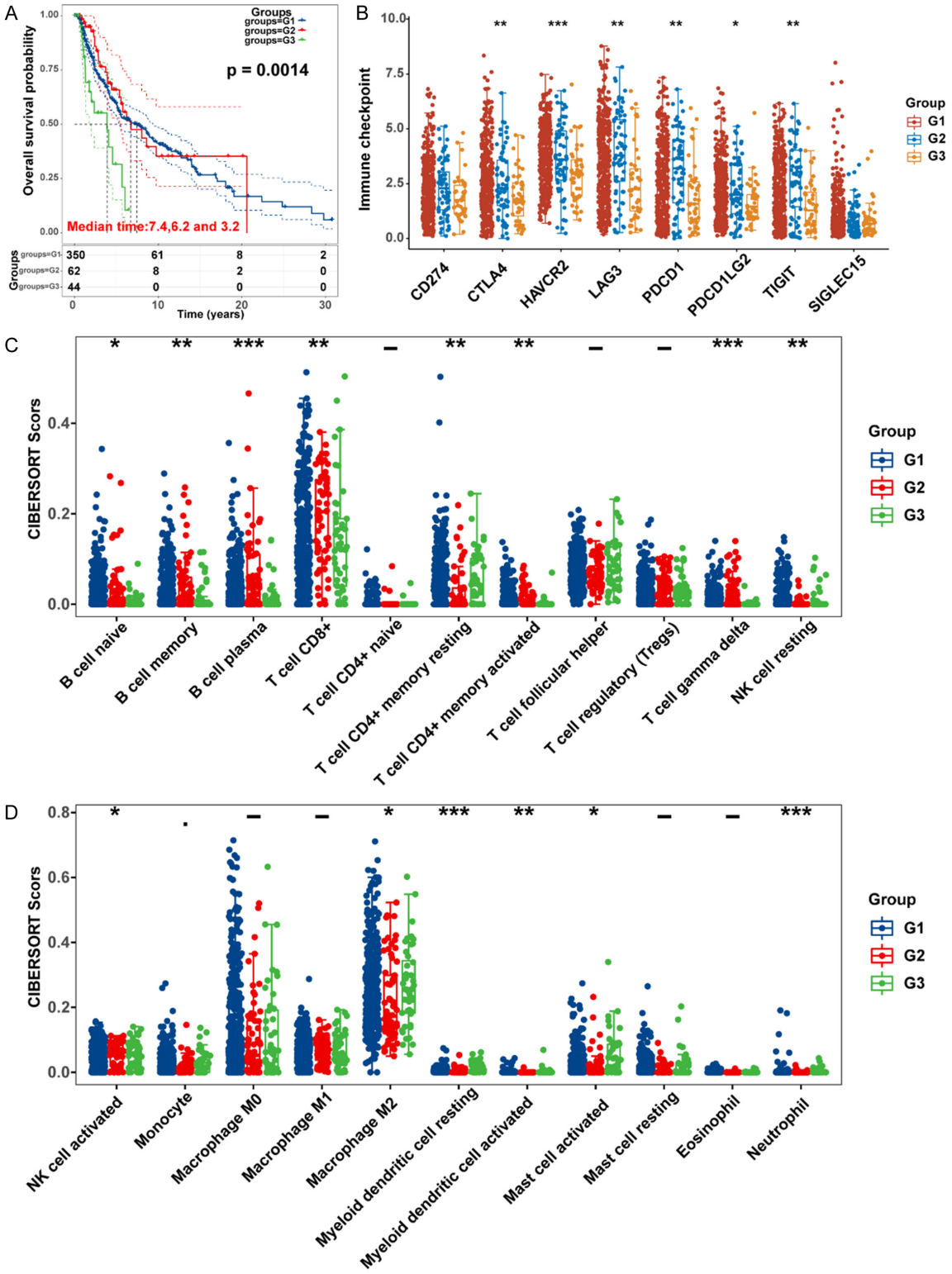

Figure 6. Immune analysis in the three molecular subtypes. A. The overall survivals of the three molecular subtypes in SKCM. B. The expression of immune checkpoints in the three molecular subtypes of SKCM. C, D. The immune scores of multiple immune cells in three molecular subtypes of SKCM.

CAPNS1 expression in A-375 and SK-MEL-28 cells after transfection of siRNAs targeting CAPNS1, and the results suggested that the knockdown efficiency of these siRNAs was high

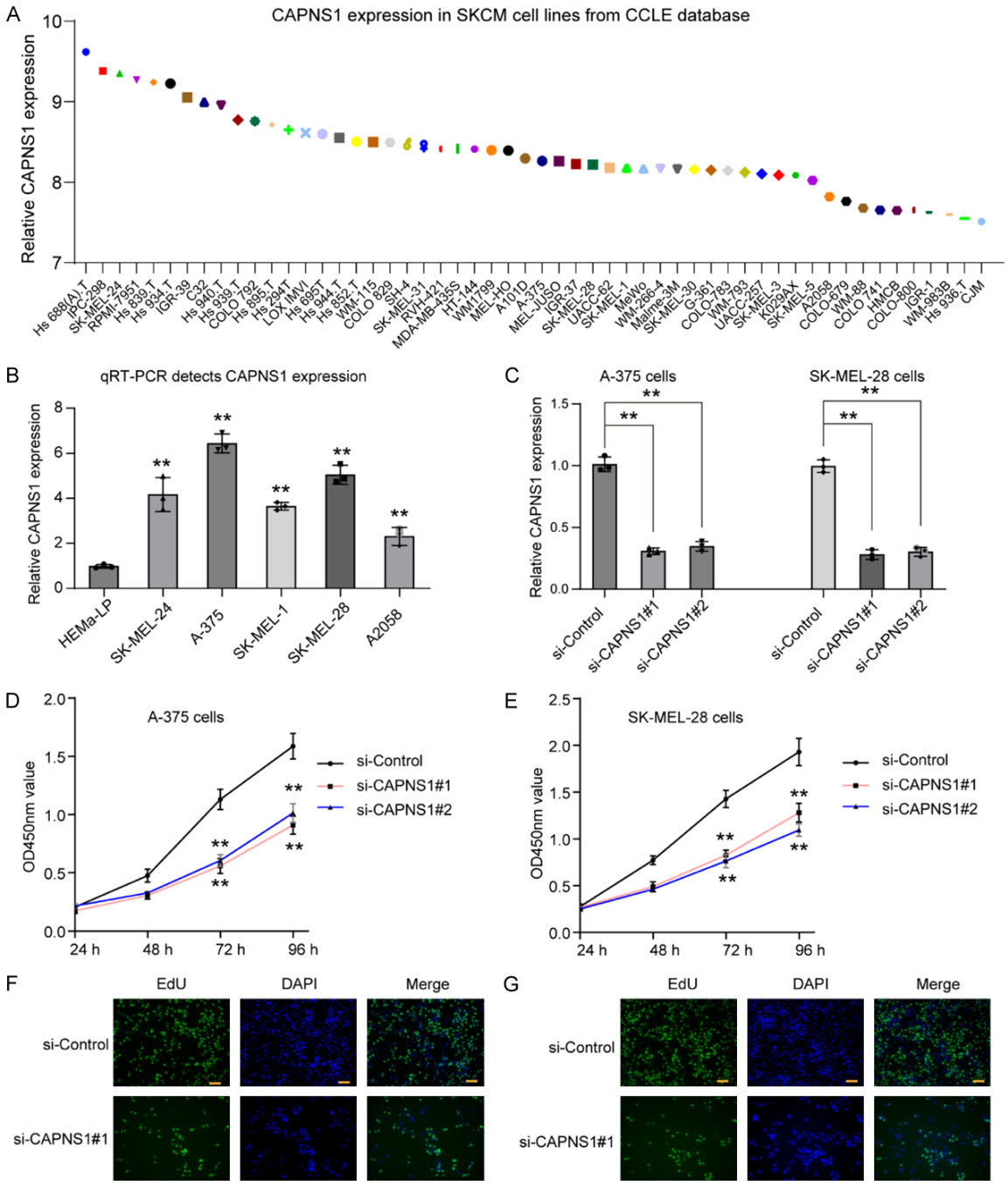

Figure 7. CAPNS1 affected melanoma cell proliferation. A. CAPNS1 expression in SKCM cell lines from CCLE database. B. The qRT-PCR detects CAPNS1 expression in melanoma cell lines. C. The qRT-PCR assays. D, E. CCK-8 assays. F, G. EdU incorporation assays. Scale bars: 20 μm. **p*-value < 0.05, ***p*-value < 0.01, ****p*-value < 0.001.

(**Figure 7C**). Afterwards, CCK-8 assays demonstrated that the depletion of CAPNS1 remarkably attenuated the proliferation of both A-375 and SK-MEL-28 cells (**Figure 7D** and **7E**). Then, EdU incorporation assays were also employed to evaluate the affection of CAPNS1 on melanoma cellular growth, and the data suggested that impeding CAPNS1 expression notably reduced the proliferate cells of both A-375 and SK-MEL-28 cells (**Figure 7F** and **7G**). Then, we performed in vivo experiments. The tumor volumes and weights in the CAPNS1-deficient group were remarkably smaller than those in the sh-control group, suggesting that repress-

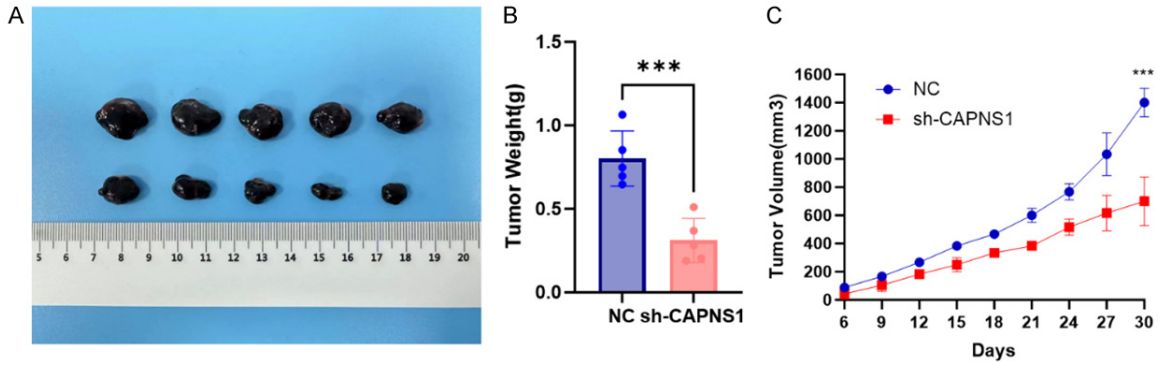

Figure 8. In vivo mice studies validated that CAPNS1 depletion suppressed tumor growth. A. Images of tumors and a size contrast to the original cells are presented. B. The tumor volume-time curves. C. The tumor weights. ***p-value < 0.001.

ing CAPNS1 expressions significantly inhibited tumor growth (**Figure 8A-C**).

CAPNS1 knockdown suppressed the metastasis and EMT of melanoma cells and promoted autophagy

Next, we set out to investigate CAPNS1's potential role in the spread of SKCM. Evidence from wound-healing experiments revealed that CAPNS1 depletion significantly slowed the rate at which A-375 and SK-MEL-28 cells healed wounds (**Figure 9A** and **9B**). Moreover, the results acquired from transwell analyses certified that suppression of CAPNS1 resulted in markedly decreased invasive cell numbers (**Figure 9C**). We then used western blotting to measure protein concentrations of EMT-related components. Protein levels of N-cadherin and vimentin were found to be significantly decreased in CAPNS1-deficient A-375 and SK-MEL-28 cells (**Figure 9D**). Finally, we confirmed that CAPNS1 knockdown promoted autophagy (**Figure 9E**).

CAPNS1 regulated Notch signaling in SKCM

Next, we wonder whether CAPNS1 might modulate signaling pathways to exert its functions in SKCM. Therefore, we first compared the expressing correlation between CAPNS1 and several classical signaling related genes in SKCM (**Figure 10A-H**). These signaling pathways were ferroptosis-related genes, m6A-relatedgnes, Notch signaling, Hedgehog signaling, JAK-STAT signaling, WNT signaling, hypoxia-related genes and mTOR signaling. The results indicated that CAPNS1 was significantly positively correlated with most genes in Notch signaling. Therefore, we sought to investigate whether CAPNS1 was able to affect Notch signaling in SKCM cells. According to the data of western blot assays, CAPNS1 knockdown dramatically silenced the protein expression of Notch signaling critical factors, Notch1, p21 and Hes1 in both A-375 and SK-MEL-28 cells (**Figure 10I** and **10J**).

Discussion

The prognosis of SKCM patients varies due to individual differences, closely linked to factors such as tumor stage, size, depth, metastasis, and genetic variations [23]. Early diagnosis and treatment play a pivotal role in improving prognosis, yet managing advanced SKCM remains challenging. Comprehensive treatment strategies may encompass surgical resection, radiation therapy, chemotherapy, and immunotherapy, aimed at prolonging survival and enhancing quality of life [24]. In the field of SKCM research, recent advancements have been focused on a deeper understanding of the tumor's molecular mechanisms and biological characteristics, in order to develop more targeted therapeutic approaches [25, 26]. The application of genome sequencing technologies empowers researchers to unveil tumor gene variations, mutations, and potential therapeutic targets. Immunotherapy has also made significant progress in SKCM treatment, such as the application of immune checkpoint inhibitors, which enhance the immune system's ability to combat tumors. Key biomarkers of current interest in SKCM research include BRAF gene mutations, particularly the V600E mutation, closely associated

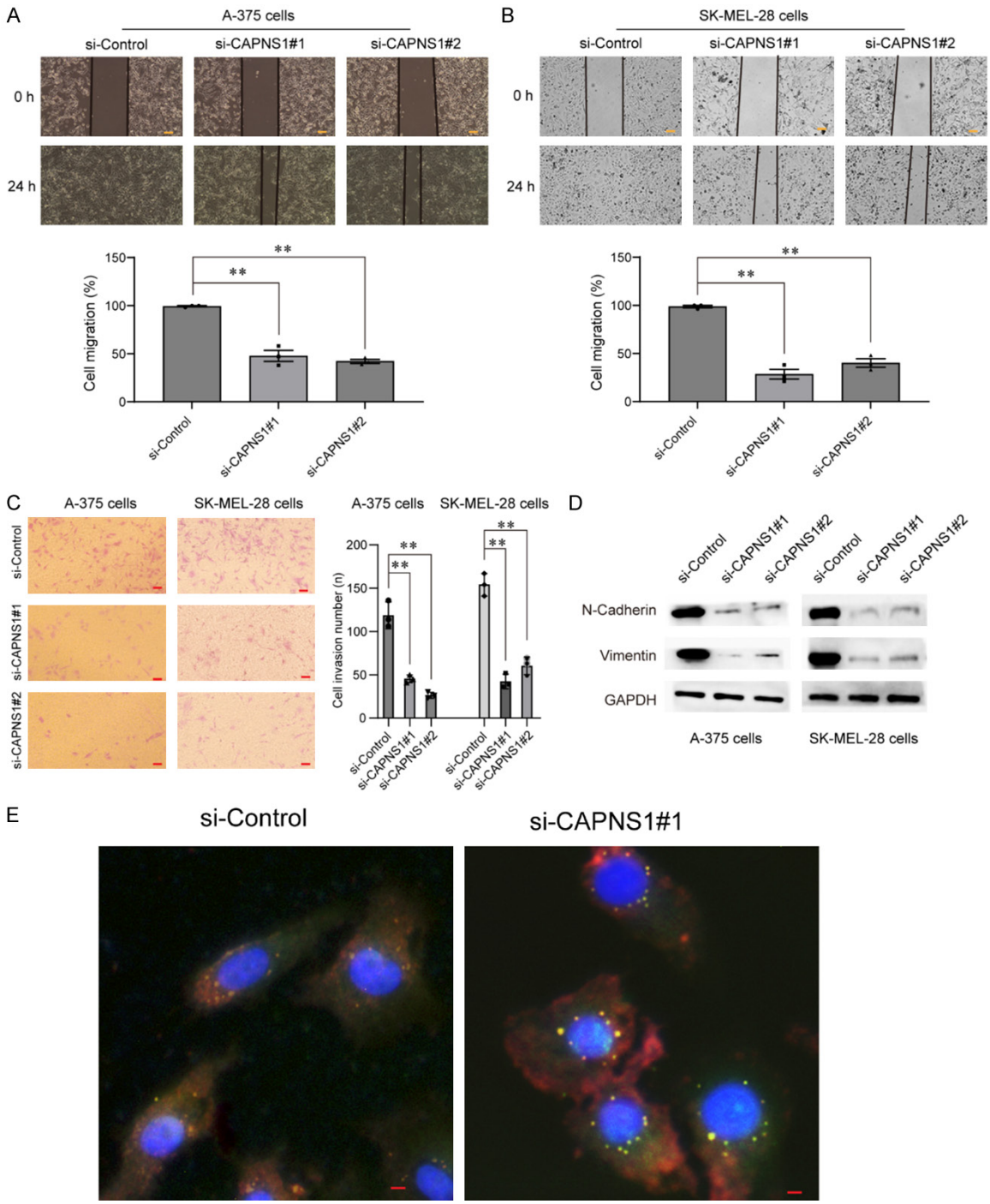

Figure 9. CAPNS1 knockdown suppressed the metastasis and EMT of melanoma cells and promoted autophagy. A and B. The migration abilities were evaluated in SKCM cells after CAPNS1 knockdown. Scale bars: 200 μm. C. Transwell assays detected the invasion capacities of SKCM cells. Scale bars: 100 μm. D. The expression of EMT-related proteins was examined in SKCM cells after CAPNS1 knockdown. E. CAPNS1 knockdown promoted autophagy.

with tumor development and prognosis. PD-L1, an immune checkpoint protein, has implications for the efficacy of immunotherapy and patient prognosis. MITF, a transcription factor, plays a pivotal role in SKCM differentiation and growth, correlating with tumor development and transformation [27, 28]. Furthermore, CTLA-4, another immune checkpoint protein, is linked to the responsiveness to immunotherapy and prognosis. SKCM tumor markers play a sig-

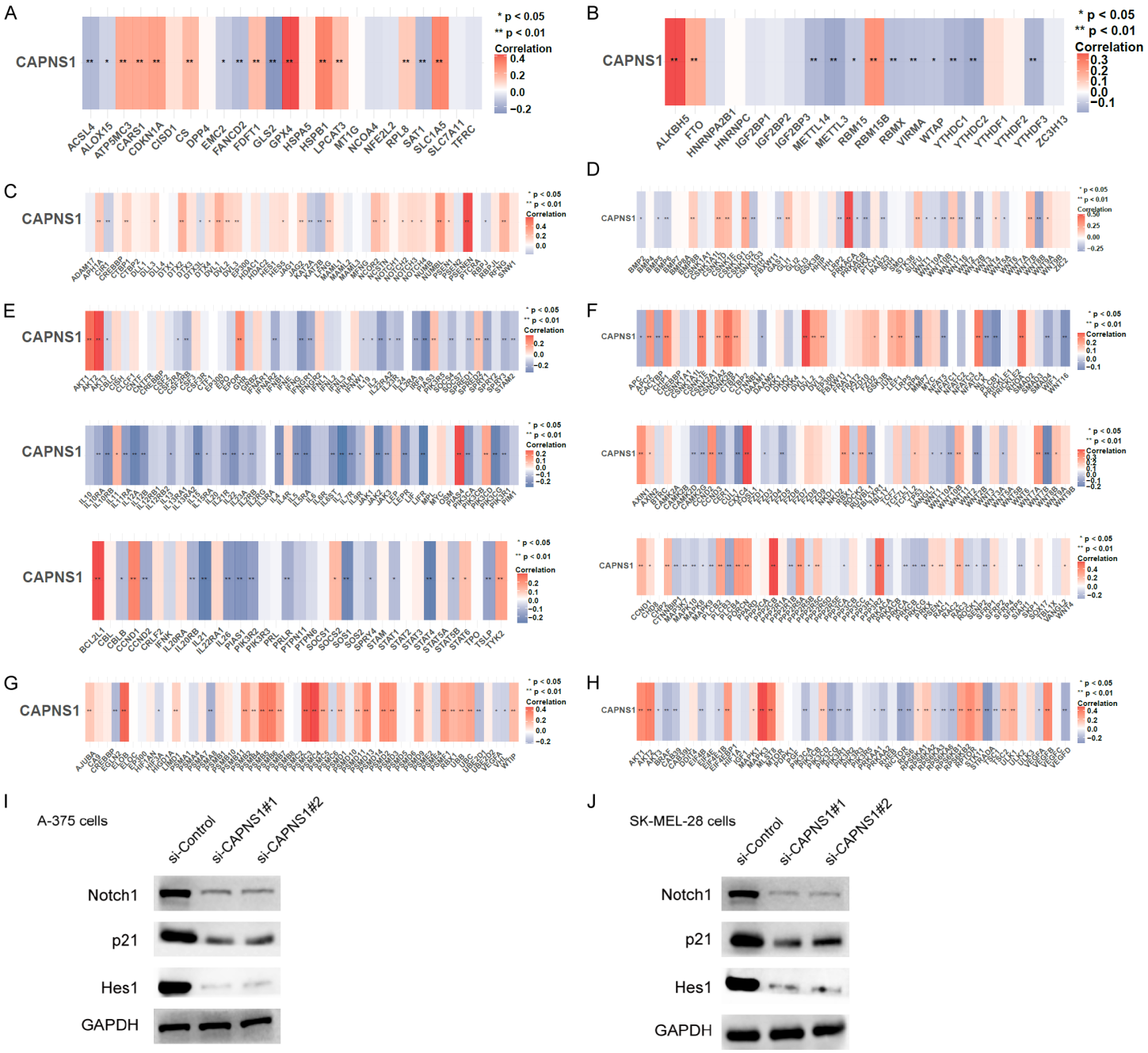
A
CAPNS1
* p < 0.05
** p < 0.01
Correlation
ACSL4 ALOX15 ATP6MC3 CARS1 CDKN1A CISD1 CS DPP4 EMC2 FANCD2 FDFT1 GLS2 GPX4 HSPA5 HSPB1 LPCAT3 MT1G NCOA4 NFE2L2 RPL8 SAT1 SLC1A5 SLC7A11 TFRC
B
CAPNS1
ALKBH5 FTO HNRNPA2B1 HNRNPC IGF2BP1 IGF2BP2 IGF2BP3 METTL14 METTL3 RBM15 RBM15B RBMX VIRMA WTAP YTHDC1 YTHDC2 YTHDF1 YTHDF2 YTHDF3 ZC3H13
C
CAPNS1
D
CAPNS1
E
CAPNS1
F
CAPNS1
G
CAPNS1
H
CAPNS1
I
A-375 cells
si-Control
si-CAPNS1#1
si-CAPNS1#2
Notch1
p21
Hes1
GAPDH
J
SK-MEL-28 cells
si-Control
si-CAPNS1#1
si-CAPNS1#2
Notch1
p21
Hes1
GAPDH

Figure 10. The correlation of CAPNS1 and multiple signalings. A. Ferroptosis-related genes. B. m6A-relatedgnes. C. Notch signaling. D. Hedgehog signaling. E. JAK-STAT signaling. F. WNT signaling. G. Hypoxia-related genes. H. mTOR signaling. I and J. Western blot assays detected the protein levels of Notch signaling critical factors, Notch1, p21 and Hes1 in both A-375 and SK-MEL-28 cells.

nificant role in clinical diagnosis and prognosis assessment, yet they also come with certain limitations. Firstly, insufficient specificity is a common issue as some markers are expressed in other tumor types or normal tissues, potentially leading to misdiagnosis. Secondly, heterogeneity and variability are also factors to consider, as genetic variations among tumor cells and environmental factors can result in differences and instability in marker expression. Additionally, some markers may only apply to specific subtypes of SKCM, rendering them inaccurate for other subtypes [29, 30]. The lack of standardized methods to evaluate marker expression and the dynamic changes of markers during the course of treatment can also impact their clinical application. Thus, more sensitive biomarkers for SKCM were necessary.

The relationship between autophagy and tumor development is complex and crucial. Autophagy is an intracellular self-degradation and recycling process that plays a dual role in tumor development, both promoting tumor growth and inhibiting it, depending on various factors [31]. In terms of promoting tumor development, autophagy can provide energy to tumor cells, regulate hormone secretion, and even play a role in drug resistance [32, 33]. However, in terms of inhibiting tumor development, autophagy has the potential for tumor suppression through processes like clearing abnormal proteins, maintaining DNA stability, and guiding cells towards autophagic cell death. Autophagy plays a crucial and complex role in the progression of SKCM (skin cancer). As an intracellular self-degradation and recycling process, autophagy can have dual effects on SKCM progression, depending on various factors such as tumor stage, cell type, and microenvironment conditions. Firstly, autophagy may promote the progression of SKCM. By providing energy and nutrients, autophagy supports the survival and proliferation of SKCM cells. Additionally, autophagy might help SKCM cells evade immune attacks or the effects of anticancer drugs, thereby fostering tumor growth and drug resistance [34, 35]. Conversely, autophagy might also suppress SKCM progression. Through clearing damaged organelles, abnormal proteins, and DNA-damaged cells, autophagy helps prevent the accumulation of abnormalities that can lead to cellular carcinogenesis. Moreover, autophagy can guide SKCM cells towards autophagic cell death, thereby limiting tumor growth. The influence of the tumor microenvironment on autophagy is also intricate. Certain microenvironmental conditions may promote autophagy, providing survival advantages to tumor cells [36]. However, in other circumstances, the microenvironment might inhibit autophagy, leading to cell death. In this study, we focused on ARGs within the context of SKCM. By analyzing DE-ARGs in SKCM, we revealed 33 up-regulated and 37 down-regulated DE-ARGs. Functional enrichment analysis demonstrated that these genes are closely associated with autophagy regulation, protein kinase activity, and ubiquitin pathways. Additionally, KEGG pathway analysis indicated their relevance to cancer-related pathways such as Autophagy-animal, Bladder cancer, and PI3K-Akt signaling pathway. In addition, our results indicated the existence of two distinct molecular subtypes of SKCM based on the expressions of 70 DE-ARGs. These subtypes are associated with significant differences in clinical characteristics, gene expression patterns, and overall survival outcomes. Group 1 demonstrates a more aggressive molecular profile, marked by higher expression of ferroptosis-related genes, m6A-related genes, and immune checkpoint genes. This aggressive profile might contribute to the unfavorable clinical outcomes observed in this group. In contrast, group 2 exhibits a more favorable prognosis, potentially indicating a less aggressive disease phenotype. The identification of these molecular subtypes and their associated differences provides valuable insights into the heterogeneity of SKCM and may aid in tailoring targeted therapies for specific subgroups. Collectively, the findings suggested that 70 DE-ARGs played a multifaceted role in SKCM progression, contributing insights into potential mechanisms underlying SKCM development and offering avenues for future therapeutic investigations.

Then, we further explored the prognostic value of 70 DE-ARGs in SKCM and screened 18 survival-related DE-ARGs including APOL1, CAPNS1, CCR2, CXCR4, EIF4EBP1, PRKCQ, RGS19, SERPINA1, BIRC5, DNAJB9, EGFR, CASP4, CFLAR, ATG9B, DAPK2, FAS, PTK6 and ULK1. In addition, our results indicated that there are intricate expression correlations and protein-protein interactions among the identified 18 survival-related DE-ARGs in SKCM. The negative correlation observed between certain DE-ARGs could imply potential regulatory relationships, indicating a complex regulatory network involving these genes in SKCM. Moreover, the identification of central nodes within the PPI network, such as BIRC5, EGFR, CFLAR, CXCR4, CCR2, and FAS, highlights their potential significance in influencing interactions among the DE-ARGs. The results of pan-cancer assays also highlighted the important roles of 18 survival-related DE-ARGs in tumor progression. Methylation is an epigenetic modification involving the addition of methyl groups to DNA molecules, typically occurring at CpG dinucleotides (cytosine and guanine connected by a phosphate backbone) [37, 38]. This chemical modification can have enduring effects on the genome, influencing gene expression and function. Methylation plays a crucial role in maintaining genome stability and regulating gene expression in normal cells [39, 40]. However, in tumors, abnormal changes in methylation can lead to misregulated gene expression, affecting normal cellular growth control, differentiation, and even promoting cancer development. In this study, we confirmed that nearly all the 18 DE-ARGs' methylation was negatively correlated with their corresponding expression in SKCM.

The tumor immune microenvironment refers to a complex network of various immune cells, cytokines, signaling molecules, and cellular interactions present within the tumor tissue [41]. It plays a crucial role in regulating the growth, spread, and therapeutic response of tumors. The composition and status of the tumor immune microenvironment have significant impacts on tumor development and patient prognosis. In the tumor immune microenvironment, immune cells play a vital role and encompass various types of immune cells such as T cells, B cells, natural killer (NK) cells, dendritic cells, and macrophages [42, 43]. These immune cells interact with tumor cells, modulating tumor growth and immune responses. Cytokines like interferons, tumor necrosis factor, and interleukins also have significant roles in the tumor immune microenvironment, influencing the activation, proliferation, and function of immune cells. The tumor immune microenvironment also involves interactions between tumor cells and the surrounding stromal cells [44, 45]. Tumor cells can secrete cytokines and signaling molecules to regulate neighboring cells and tissues, promoting tumor growth and invasion. Additionally, the tumor immune microenvironment includes immune checkpoint molecules that regulate the activity of immune cells, impacting the strength and duration of the immune response. In this study, we found that the 18 DE-ARGs were dramatically related with kinds of immune cells such as NK cell, Macrophage, Endothelial cell, T cells, B cell. Our results suggested that 18 DE-ARGs may be involved in regulating the activity and function of immune cells, thereby influencing the formation and development of the tumor immune microenvironment. These genes may impact immune cell activation, proliferation, differentiation, and regulation through different pathways, further influencing the tumor's immune response and progression. This discovery provides clues for further investigating the role of autophagy in the tumor immune microenvironment and offers potential targets for the development of new tumor immunotherapies.

Gene signatures derived from transcriptome analyses have great promise as a tool for tracking tumors' prognostic risks. This method involves analyzing the gene expression characteristics of tumor cells to identify a set of gene markers associated with specific cancers. These markers can be used to predict the prognosis of patients. The purpose of this method is to provide information about the potential disease progression and survival rates of cancer patients through gene expression data, guiding clinical treatment and decisions. This approach holds significant importance for the development of personalized medicine and precision therapy. Previously, several studies have developed novel prognostic signature based on ARGs in many types of tumors, such as lung cancer, prostate cancer and glioma [46-48]. However, the ARGs-related signature in SKCM was rarely reported. In this study, we used

LASSO Cox regression analysis to establish a risk profile for autophagy, which consists of 12 OS-related ARGs. High-risk patients' overall survival times were dramatically lower than those of low-risk patients. Based on the results, our prognostic signature of ARGs exhibited a significant negative correlation with various immune cell types in SKCM, including B cells, CD4+ T cells, CD8+ T cells, neutrophils, macrophages, and myeloid dendritic cells. This observation suggests a potential association between our ARGs prognostic signature and the activity and functions of these immune cell types within the SKCM microenvironment. The negative correlation implies that the regulation of immune cells might be influenced by the ARGs signature, potentially impacting the tumor immune microenvironment and further influencing the progression of the tumor and the prognosis of patients. These findings provide valuable insights for further exploring the role of autophagy in the tumor immune microenvironment.

Among 12 OS-related ARGs, our attention focused on CAPNS1 because its function in SKCM was rarely reported. CAPNS1 (Calpain Small Subunit 1) is a gene that encodes a protein involved in regulating actin, a major protein component of the cell's cytoskeleton [49]. The protein encoded by CAPNS1 is the small subunit of the Calpain enzyme complex, which, when combined with the large subunit, forms the active Calpain enzyme complex. Calpains are a class of calcium-dependent proteases that play a role in various cellular processes such as membrane protein cleavage, cell migration, apoptosis, and signal transduction [50, 51]. The product of CAPNS1 is crucial for regulating the activity and function of the Calpain enzyme complex in the context of actin regulation. In the field of cancer research, CAPNS1 may be linked to the development and progression of certain cancers. Some studies suggest that abnormal expression of CAPNS1 in certain tumors could be associated with phenomena such as tumor cell proliferation, migration, and invasion. For instance, Zhuang et al reported that the expression of CAPNS1 was significantly elevated in renal cell carcinoma tissues compared to adjacent non-tumor tissues. Multivariate analysis demonstrated that CAPNS1 overexpression served as an independent unfavorable prognostic indicator in renal cell carcinoma. In vitro experiments showed that silencing the CAPNS1 gene hindered cell adhesion and impaired the migratory and invasive abilities of renal cell carcinoma cells. Furthermore, the suppression of CAPNS1 expression led to decreased levels of MMP2 and MMP9 expression. A comprehensive analysis of these findings suggests that the heightened expression of the CAPNS1 in renal cell carcinoma is associated with poor prognosis. The gene's silencing resulted in inhibitory effects on cell adhesion, migration, and invasion, while also influencing the expression of genes linked to tumor-related processes. In this study, we found that CAPNS1 was highly expressed in SKCM specimens and cells. Survival assays revealed that high CAPNS1 expression predicted a poor prognosis of SKCM patients. Moreover, we confirmed that CAPNS1 knockdown promoted autophagy. CAPNS1 is a protease, and its function in the cell is associated with the process of autophagy. Autophagy is a crucial metabolic process within cells, where damaged or unneeded organelles and proteins are degraded and recycled. CAPNS1 plays a regulatory and facilitating role in the autophagy process [10, 52]. Research indicates that CAPNS1 is involved in the regulation and execution of autophagy. It can interact with other proteins, forming complexes that regulate signaling pathways related to autophagy [51, 53]. Additionally, CAPNS1 may directly participate in the degradation process of autophagy-related proteins, helping to maintain cellular autophagic balance. Our findings firstly provided evidences that CAPNS1 knockdown promoted autophagy. In addition, we found that CAPNS1 demonstrated positive correlations with specific immune cells, such as natural killer (NK) cells, γδT cells, macrophages, dendritic cells (DC), and the overall immune infiltration score. Conversely, CAPNS1 exhibited negative correlations with other immune cell types, including nTreg (natural regulatory T cells), central memory infiltration, induced regulatory T cells (iTreg), and CD4 naive infiltration. These findings suggest that CAPNS1 may play a multifaceted role in shaping the immune microenvironment of tumors. The positive correlations with certain immune cells imply its potential involvement in promoting immune responses, while negative correlations might point towards immunosuppressive effects. The complex interactions highlighted in the immune interaction

network suggest that CAPNS1 might contribute to the regulation of immune cell activities, which can impact tumor progression, immunosurveillance, and therapeutic responses.

Finally, to determine CAPNS1's possible role in SKCM, we conducted in vitro tests and discovered that CAPNS1 knockdown suppressed the proliferation, metastasis and EMT of melanoma cells and promoted autophagy. We found that CAPNS1 was significantly positively correlated with most genes in Notch signaling. The Notch signaling pathway is a highly conserved and widely present cellular signaling pathway in various organisms, playing a crucial role in normal embryonic development, cell fate determination, and tissue maintenance [54]. However, recent research indicates that the Notch signaling pathway also plays an important role in tumor development and progression. The Notch signaling pathway is activated by the binding of Notch receptors to their ligands, such as Delta and Jagged. This binding leads to the intracellular domain of the Notch receptor undergoing enzymatic cleavage, releasing active transcription factors that subsequently influence the expression of downstream genes [55]. The Notch signaling system is essential for the regulation of events essential to proper cell function, including cell differentiation, proliferation, and death in normal cells. However, in tumors, abnormal activation or inhibition of the Notch pathway may lead to abnormal cell proliferation, survival, and metastasis [56]. Therefore, we sought to investigate whether CAPNS1 was able to affect Notch signaling in SKCM cells. Importantly, we confirmed that CAPNS1 knockdown dramatically silenced the protein expression of Notch signaling critical factors, Notch1, p21 and Hes1 in both A-375 and SK-MEL-28 cells. Notch1 is a major component of the Notch signaling pathway, while p21 and Hes1 are downstream genes regulated by the Notch signaling pathway. Therefore, the reduced protein expression of these key factors following CAPNS1 knockdown may suggest that CAPNS1 plays a significant role in modulating the activity of the Notch signaling pathway. This finding may offer insights into a better understanding of the role of CAPNS1 in cellular signaling regulation and tumor development. Additionally, it could provide guidance for future research exploring the interplay between CAPNS1 and the Notch signaling pathway, as well as their potential implications in tumor therapy.

Several caveats inherent to our study merit careful consideration. Firstly, our research relied heavily on data obtained from TCGA, in which the majority of patients were either White or Asian. To improve the generalizability of our findings, it's necessary to conduct additional research involving more diverse patient populations. This could involve collaborating with researchers who specialize in specific ethnic groups or expanding the scope of your study to include a broader range of participants. Secondly, our study focused on investigating the potential functional implications of CAPNS1 in the progression of malignant SKCM through in vitro experimentation. The in vitro experiments allowed us to gain initial insights into the role of CAPNS1 in SKCM. However, to provide a comprehensive understanding of CAPNS1's significance in SKCM, it is imperative to extend our investigations to in vivo settings.

Conclusion

We systematically screened a panel of 18 pivotal autophagy-related genes (ARGs) implicated in the progression of malignant melanoma. Through rigorous analysis, we have successfully delineated a novel autophagy-related gene signature. This signature emerges as a valuable tool for prognostic assessment among patients afflicted with SKCM. By integrating the intricate interplay of these identified ARGs, our study introduces a refined prognostic model that holds promise for enhancing the precision of prognostic evaluations in the context of SKCM. In addition, we identified a novel SKCM-related gene CAPNS1 which was highly expressed in SKCM patients and predicted a poor prognosis. Importantly, we confirmed that knockdown of CAPNS1 distinctly suppressed the proliferation of SKCM cells via regulating Notch signaling pathway. These results collectively contribute to our understanding of the intricate molecular interactions underlying SKCM progression and offer promising avenues for future research and clinical applications.

Acknowledgements

This work was supported by Anhui High Education Institution (No: 2022AH051500), Anhui High Education Institution (No: 2022AH-050670) and Research Foundation of Anhui Medical University (No: 2022xkj053). And

Natural Science Foundation of Bengbu Medical University (No: 2023byzd118).

Disclosure of conflict of interest

None.

Address correspondence to: Jiabin Deng, Department of Burn and Plastic Surgery, The Third People's Hospital of Bengbu, No. 38, Shengli Middle Road, Shengli Street, Bengshan District, Bengbu 233000, Anhui, China. E-mail: dengjiabin1028@163.com

References

[1] Leonardi GC, Falzone L, Salemi R, Zanghì A, Spandidos DA, McCubrey JA, Candido S and Libra M. Cutaneous melanoma: from pathogenesis to therapy (Review). Int J Oncol 2018; 52: 1071-1080.

[2] Hartman RI and Lin JY. Cutaneous melanoma-a review in detection, staging, and management. Hematol Oncol Clin North Am 2019; 33: 25-38.

[3] Tímár J and Ladányi A. Molecular pathology of skin melanoma: epidemiology, differential diagnostics, prognosis and therapy prediction. Int J Mol Sci 2022; 23: 5384.

[4] Schadendorf D, van Akkooi ACJ, Berking C, Griewank KG, Gutzmer R, Hauschild A, Stang A, Roesch A and Ugurel S. Melanoma. Lancet 2018; 392: 971-984.

[5] Cabrera R and Recule F. Unusual clinical presentations of malignant melanoma: a review of clinical and histologic features with special emphasis on dermatoscopic findings. Am J Clin Dermatol 2018; 19 Suppl 1: 15-23.

[6] Maibach F, Sadozai H, Seyed Jafari SM, Hunger RE and Schenk M. Tumor-infiltrating lymphocytes and their prognostic value in cutaneous melanoma. Front Immunol 2020; 11: 2105.

[7] D'Arcy MS. Cell death: a review of the major forms of apoptosis, necrosis and autophagy. Cell Biol Int 2019; 43: 582-592.

[8] Levy JMM, Towers CG and Thorburn A. Targeting autophagy in cancer. Nat Rev Cancer 2017; 17: 528-542.

[9] Parzych KR and Klionsky DJ. An overview of autophagy: morphology, mechanism, and regulation. Antioxid Redox Signal 2014; 20: 460-473.

[10] Mizushima N and Komatsu M. Autophagy: renovation of cells and tissues. Cell 2011; 147: 728-741.

[11] Filomeni G, De Zio D and Cecconi F. Oxidative stress and autophagy: the clash between damage and metabolic needs. Cell Death Differ 2015; 22: 377-388.

[12] Kuma A, Komatsu M and Mizushima N. Autophagy-monitoring and autophagy-deficient mice. Autophagy 2017; 13: 1619-1628.

[13] Li W, He P, Huang Y, Li YF, Lu J, Li M, Kurihara H, Luo Z, Meng T, Onishi M, Ma C, Jiang L, Hu Y, Gong Q, Zhu D, Xu Y, Liu R, Liu L, Yi C, Zhu Y, Ma N, Okamoto K, Xie Z, Liu J, He RR and Feng D. Selective autophagy of intracellular organelles: recent research advances. Theranostics 2021; 11: 222-256.

[14] Kocaturk NM, Akkoc Y, Kig C, Bayraktar O, Gozuacik D and Kutlu O. Autophagy as a molecular target for cancer treatment. Eur J Pharm Sci 2019; 134: 116-137.

[15] Pai JA and Satpathy AT. High-throughput and single-cell T cell receptor sequencing technologies. Nat Methods 2021; 18: 881-892.

[16] Reuter JA, Spacek DV and Snyder MP. High-throughput sequencing technologies. Mol Cell 2015; 58: 586-597.

[17] Pareek CS, Smoczynski R and Tretyn A. Sequencing technologies and genome sequencing. J Appl Genet 2011; 52: 413-435.

[18] Levy SE and Boone BE. Next-generation sequencing strategies. Cold Spring Harb Perspect Med 2019; 9: a025791.

[19] Dorado G, Gálvez S, Rosales TE, Vásquez VF and Hernández P. Analyzing modern biomolecules: the revolution of nucleic-acid sequencing - review. Biomolecules 2021; 11: 1111.

[20] Xu J, Liao K, Yang X, Wu C and Wu W. Using single-cell sequencing technology to detect circulating tumor cells in solid tumors. Mol Cancer 2021; 20: 104.

[21] Shi Y, Wang G, Lau HC and Yu J. Metagenomic sequencing for microbial DNA in human samples: emerging technological advances. Int J Mol Sci 2022; 23: 2181.

[22] Kebschull JM. DNA sequencing in high-throughput neuroanatomy. J Chem Neuroanat 2019; 100: 101653.

[23] Rastrelli M, Tropea S, Rossi CR and Alaibac M. Melanoma: epidemiology, risk factors, pathogenesis, diagnosis and classification. In Vivo 2014; 28: 1005-1011.

[24] Teixido C, Castillo P, Martinez-Vila C, Arance A and Alos L. Molecular markers and targets in melanoma. Cells 2021; 10: 2320.

[25] Chattopadhyay C, Kim DW, Gombos DS, Oba J, Qin Y, Williams MD, Esmaeli B, Grimm EA, Wargo JA, Woodman SE and Patel SP. Uveal melanoma: from diagnosis to treatment and the science in between. Cancer 2016; 122: 2299-2312.

[26] Eddy K and Chen S. Overcoming immune evasion in melanoma. Int J Mol Sci 2020; 21: 8984.

[27] Pavri SN, Clune J, Ariyan S and Narayan D. Malignant melanoma: beyond the basics. Plast Reconstr Surg 2016; 138: 330e-340e.

[28] Slominski A, Wortsman J, Carlson AJ, Matsuoka LY, Balch CM and Mihm MC. Malignant melanoma. Arch Pathol Lab Med 2001; 125: 1295-1306.
[29] Abbas O, Miller DD and Bhawan J. Cutaneous malignant melanoma: update on diagnostic and prognostic biomarkers. Am J Dermatopathol 2014; 36: 363-379.
[30] Cho KK, Cust AE, Foo YM, Long GV, Menzies AM and Eslick GD. Metastatic acral melanoma treatment outcomes: a systematic review and meta-analysis. Melanoma Res 2021; 31: 482-486.
[31] Levine B and Kroemer G. Biological functions of autophagy genes: a disease perspective. Cell 2019; 176: 11-42.
[32] Klionsky DJ, Petroni G, Amaravadi RK, Baehrecke EH, Ballabio A, Boya P, Bravo-San Pedro JM, Cadwell K, Cecconi F, Choi AMK, Choi ME, Chu CT, Codogno P, Colombo MI, Cuervo AM, Deretic V, Dikic I, Elazar Z, Eskelinen EL, Fimia GM, Gewirtz DA, Green DR, Hansen M, Jäättelä M, Johansen T, Juhász G, Karantza V, Kraft C, Kroemer G, Ktistakis NT, Kumar S, Lopez-Otin C, Macleod KF, Madeo F, Martinez J, Meléndez A, Mizushima N, Münz C, Penninger JM, Perera RM, Piacentini M, Reggiori F, Rubinsztein DC, Ryan KM, Sadoshima J, Santambrogio L, Scorrano L, Simon HU, Simon AK, Simonsen A, Stolz A, Tavernarakis N, Tooze SA, Yoshimori T, Yuan J, Yue Z, Zhong Q, Galluzzi L and Pietrocola F. Autophagy in major human diseases. EMBO J 2021; 40: e108863.
[33] Kumariya S, Ubba V, Jha RK and Gayen JR. Autophagy in ovary and polycystic ovary syndrome: role, dispute and future perspective. Autophagy 2021; 17: 2706-2733.
[34] Zhang X, Li H, Liu C and Yuan X. Role of ROS-mediated autophagy in melanoma (Review). Mol Med Rep 2022; 26: 303.
[35] Ashrafizadeh M, Mohammadinejad R, Tavakol S, Ahmadi Z, Roomiani S and Katebi M. Autophagy, anoikis, ferroptosis, necroptosis, and endoplasmic reticulum stress: potential applications in melanoma therapy. J Cell Physiol 2019; 234: 19471-19479.
[36] Rahmati M, Ebrahim S, Hashemi S, Motamedi M and Moosavi MA. New insights on the role of autophagy in the pathogenesis and treatment of melanoma. Mol Biol Rep 2020; 47: 9021-9032.
[37] Moore LD, Le T and Fan G. DNA methylation and its basic function. Neuropsychopharmacology 2013; 38: 23-38.
[38] Yang B, Wang JQ, Tan Y, Yuan R, Chen ZS and Zou C. RNA methylation and cancer treatment. Pharmacol Res 2021; 174: 105937.
[39] Meng H, Cao Y, Qin J, Song X, Zhang Q, Shi Y and Cao L. DNA methylation, its mediators and genome integrity. Int J Biol Sci 2015; 11: 604-617.
[40] Perez E and Capper D. Invited review: DNA methylation-based classification of paediatric brain tumours. Neuropathol Appl Neurobiol 2020; 46: 28-47.
[41] Gajewski TF, Schreiber H and Fu YX. Innate and adaptive immune cells in the tumor microenvironment. Nat Immunol 2013; 14: 1014-1022.
[42] Lei X, Lei Y, Li JK, Du WX, Li RG, Yang J, Li J, Li F and Tan HB. Immune cells within the tumor microenvironment: biological functions and roles in cancer immunotherapy. Cancer Lett 2020; 470: 126-133.
[43] Lv B, Wang Y, Ma D, Cheng W, Liu J, Yong T, Chen H and Wang C. Immunotherapy: reshape the tumor immune microenvironment. Front Immunol 2022; 13: 844142.
[44] Marzagalli M, Ebelt ND and Manuel ER. Unraveling the crosstalk between melanoma and immune cells in the tumor microenvironment. Semin Cancer Biol 2019; 59: 236-250.
[45] Ozga AJ, Chow MT and Luster AD. Chemokines and the immune response to cancer. Immunity 2021; 54: 859-874.
[46] Diao X, Guo C and Li S. Identification of a novel anoikis-related gene signature to predict prognosis and tumor microenvironment in lung adenocarcinoma. Thorac Cancer 2023; 14: 320-330.
[47] Hu D, Jiang L, Luo S, Zhao X, Hu H, Zhao G and Tang W. Development of an autophagy-related gene expression signature for prognosis prediction in prostate cancer patients. J Transl Med 2020; 18: 160.
[48] Feng S, Liu H, Dong X, Du P, Guo H and Pang Q. Identification and validation of an autophagy-related signature for predicting survival in lower-grade glioma. Bioengineered 2021; 12: 9692-9708.
[49] Pamonsinlapatham P, Gril B, Dufour S, Hadj-Slimane R, Gigoux V, Pethe S, L'Hoste S, Camonis J, Garbay C, Raynaud F and Vidal M. Capns1, a new binding partner of RasGAP-SH3 domain in K-Ras(V12) oncogenic cells: modulation of cell survival and migration. Cell Signal 2008; 20: 2119-2126.
[50] Zhang L, Zheng D, Yan Y, Yu Y, Chen R, Li Z, Greer PA, Peng T and Wang Q. Myeloid cell-specific deletion of Capns1 prevents macrophage polarization toward the M1 phenotype and reduces interstitial lung disease in the bleomycin model of systemic sclerosis. Arthritis Res Ther 2022; 24: 148.
[51] Cataldo F, Peche LY, Klaric E, Brancolini C, Myers MP, Demarchi F and Schneider C. CAPNS1 regulates USP1 stability and maintenance of genome integrity. Mol Cell Biol 2013; 33: 2485-2496.

[52] Glick D, Barth S and Macleod KF. Autophagy: cellular and molecular mechanisms. J Pathol 2010; 221: 3-12.
[53] Marcassa E, Raimondi M, Anwar T, Eskelinen EL, Myers MP, Triolo G, Schneider C and Demarchi F. Calpain mobilizes Atg9/Bif-1 vesicles from Golgi stacks upon autophagy induction by thapsigargin. Biol Open 2017; 6: 551-562.
[54] Zhou B, Lin W, Long Y, Yang Y, Zhang H, Wu K and Chu Q. Notch signaling pathway: architecture, disease, and therapeutics. Signal Transduct Target Ther 2022; 7: 95.
[55] Sprinzak D and Blacklow SC. Biophysics of Notch signaling. Annu Rev Biophys 2021; 50: 157-189.
[56] Borggrefe T and Oswald F. The Notch signaling pathway: transcriptional regulation at Notch target genes. Cell Mol Life Sci 2009; 66: 1631-1646.

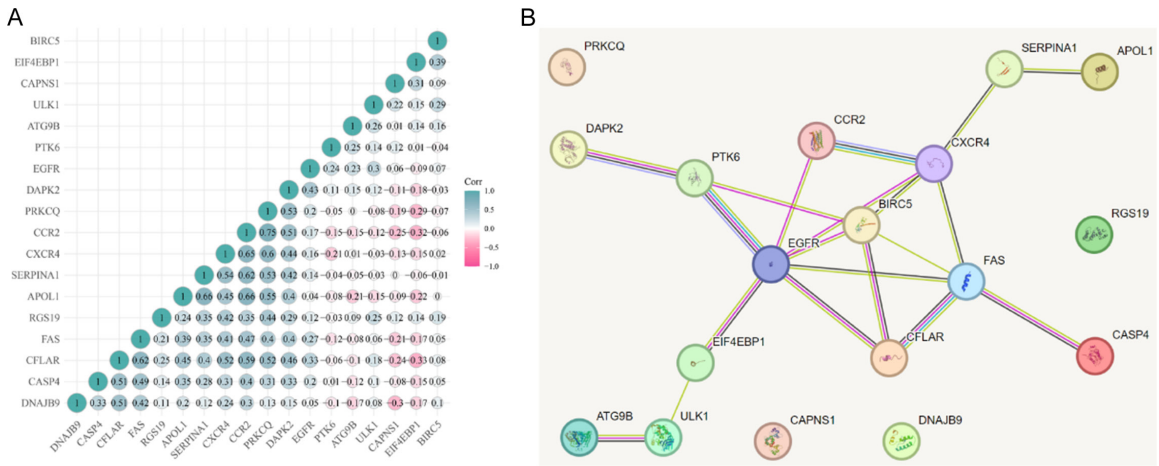

Figure S1. Gene correlation and PPI network. A. The heatmap of the correlation between the 18 DE-ARGs in 471 SKCM samples. B. Protein-protein interacting (PPI) network was generated by using STRING database.

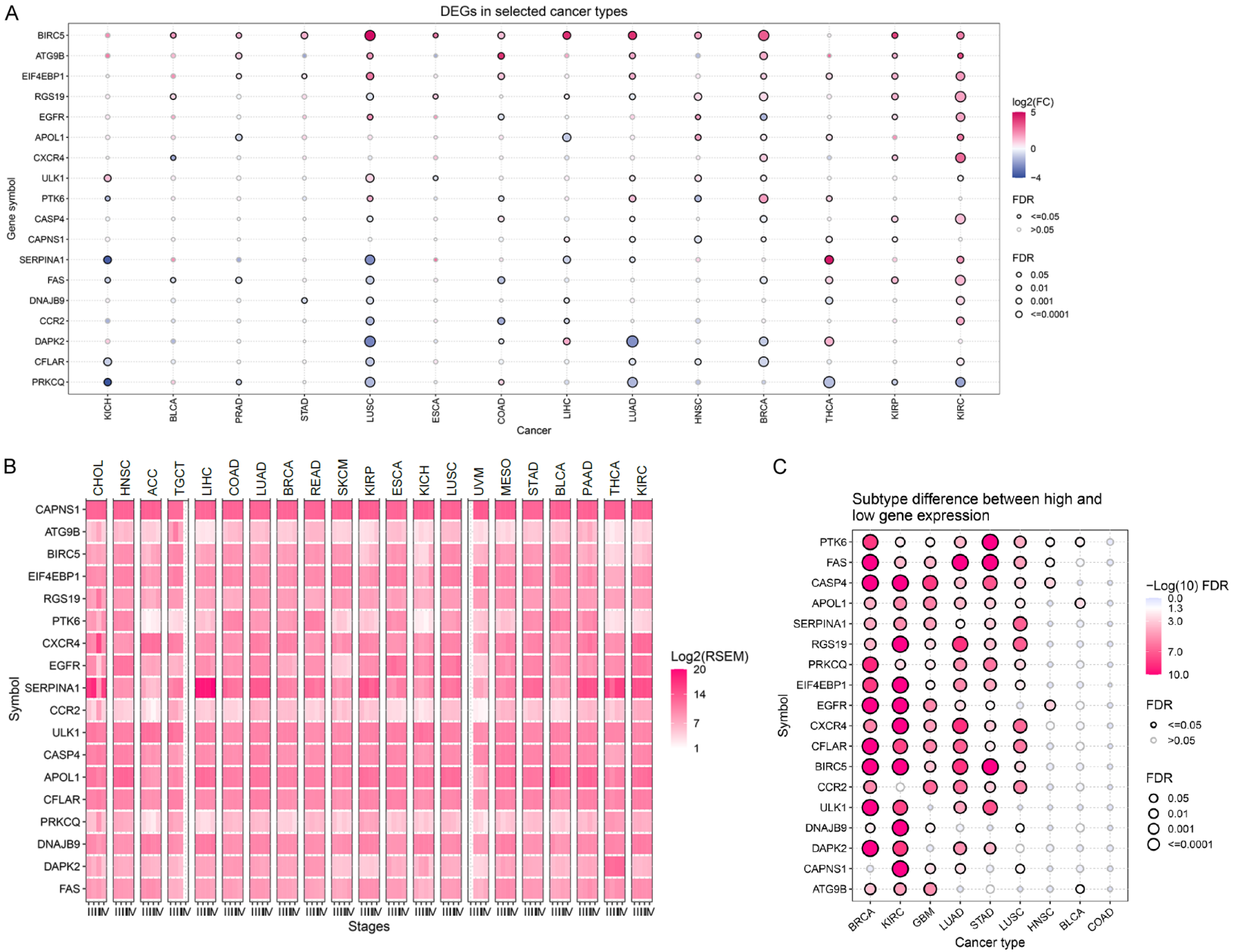
A
DEGs in selected cancer types
Gene symbol
BIRC5
ATG9B
EIF4EBP1
RGS19
EGFR
APOL1
CXCR4
ULK1
PTK6
CASP4
CAPNS1
SERPINA1
FAS
DNAJB9
CCR2
DAPK2
CFLAR
PRKCQ
KICH
BLCA
PRAD
STAD
LUSC
ESCA
COAD
LIHC
LUAD
HNSC
BRCA
THCA
KIRP
KIRC
Cancer
log2(FC)
5
0
−4
FDR
<=0.05
>0.05
FDR
0.05
0.01
0.001
<=0.0001
B
CHOL
HNSC
ACC
TGCT
LIHC
COAD
LUAD
BRCA
READ
SKCM
KIRP
ESCA
KICH
LUSC
UVM
MESO
STAD
BLCA
PAAD
THCA
KIRC
Symbol
Stages
Log2(RSEM)
20
14
7
1
C
Subtype difference between high and low gene expression
Symbol
Cancer type
BRCA
KIRC
GBM
LUAD
STAD
LUSC
HNSC
BLCA
COAD
−Log(10) FDR
0.0
1.3
3.0
7.0
10.0
FDR
<=0.05
>0.05
FDR
0.05
0.01
0.001
<=0.0001

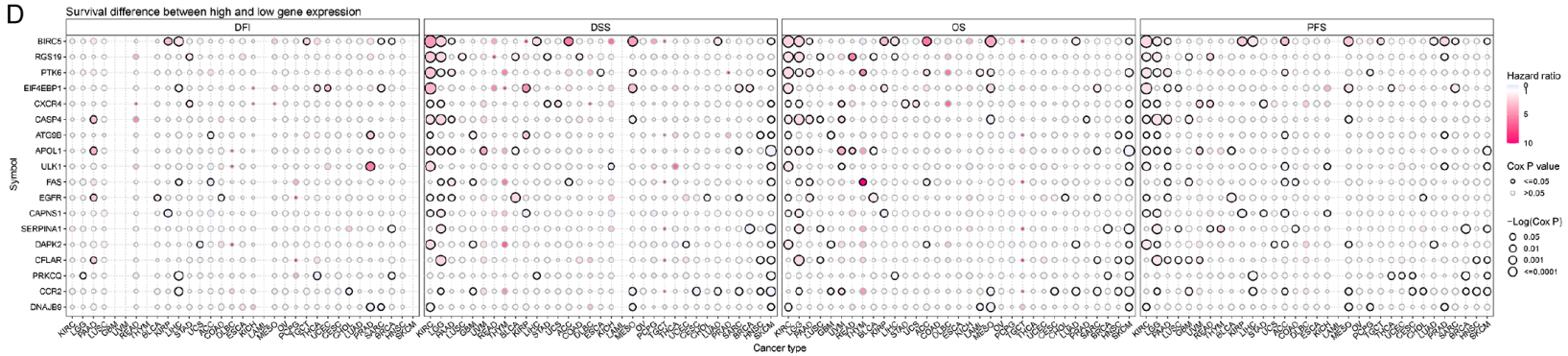

Figure S2. Expression and survival analysis. A. The expression of 18 DE-ARGs in pan-cancers. B. The 18 DE-ARGs expression in pathologic stages of pan-cancers. C. The subtype difference of pan-cancers between high and low gene expression of the 18 DE-ARGs. D. The analysis of survivals including OS, PFS, DSS and DFI in pan-cancers.

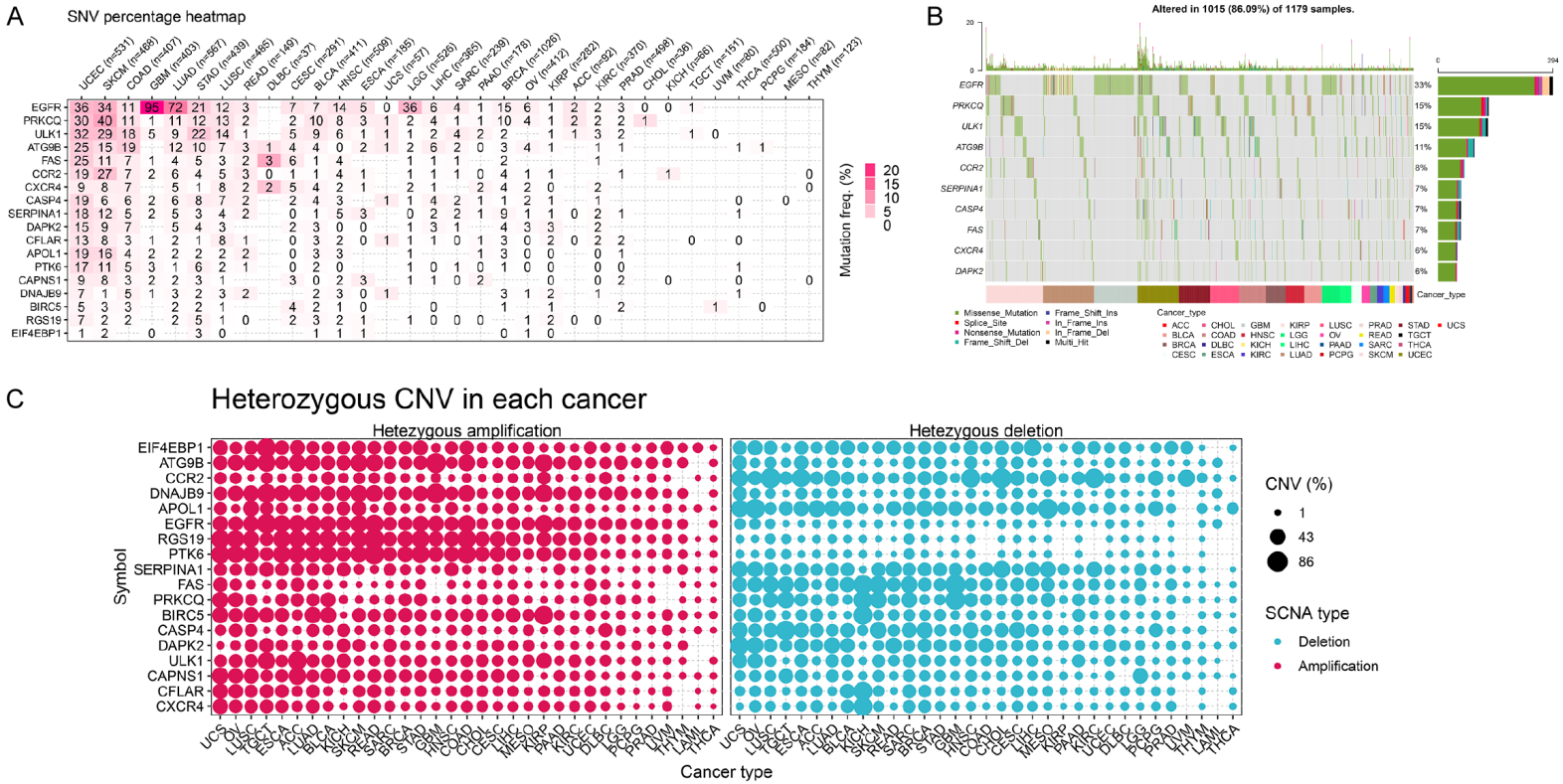

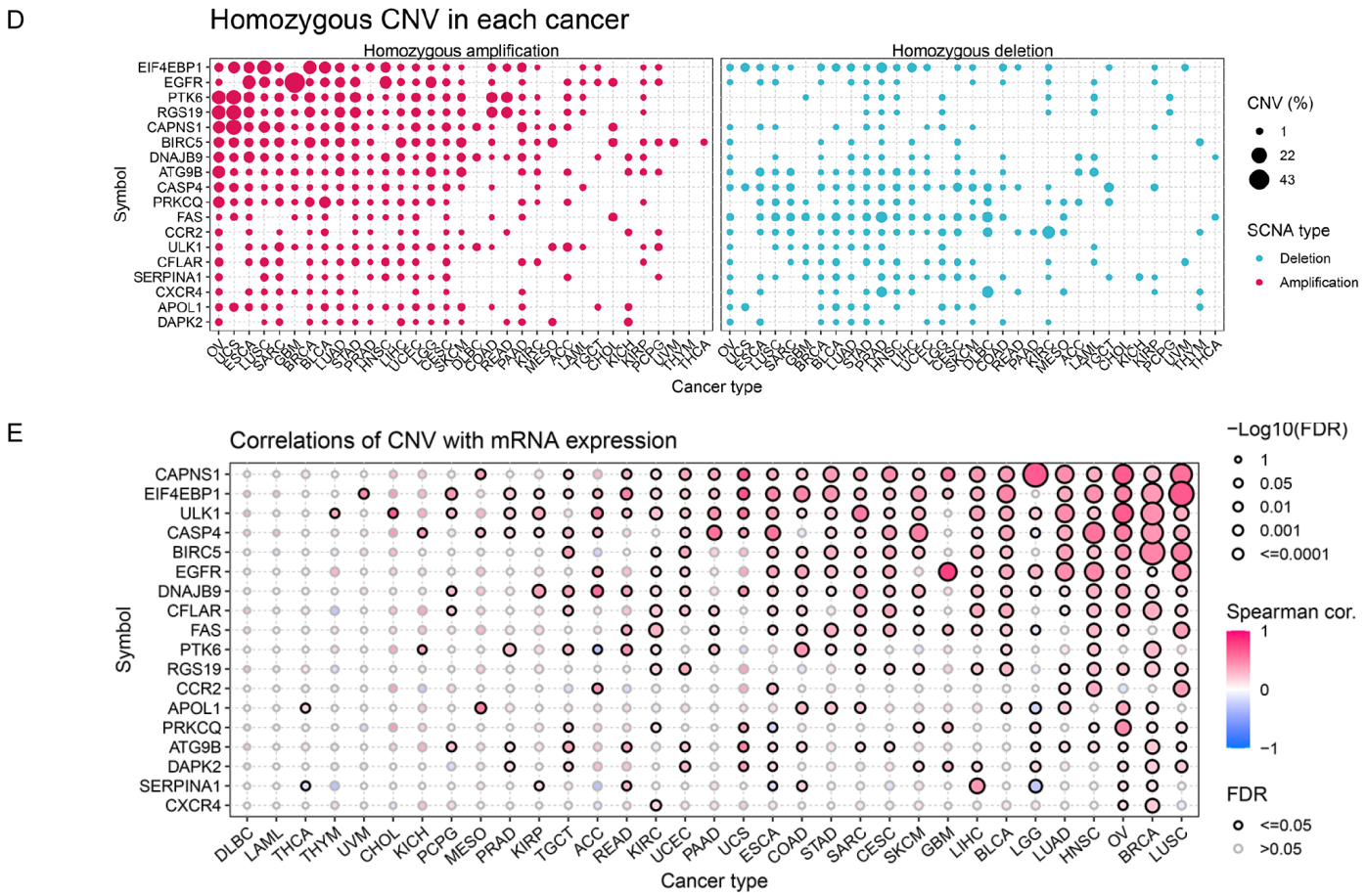

Figure S3. SNV and CNV analysis. A. The SNV (single nucleotide variants) percentage heatmap in pan-cancers. B. The waterfall plot displayed the top 10 mutated genes in pan-cancers. C and D. The CNV (copy number variation) analysis in pan-cancers including heterozygous amplification, homozygous amplification, heterozygous deletion, homozygous deletion. E. The correlation of CNV and the 18 DE-ARGs expression in TCGA cancer types.

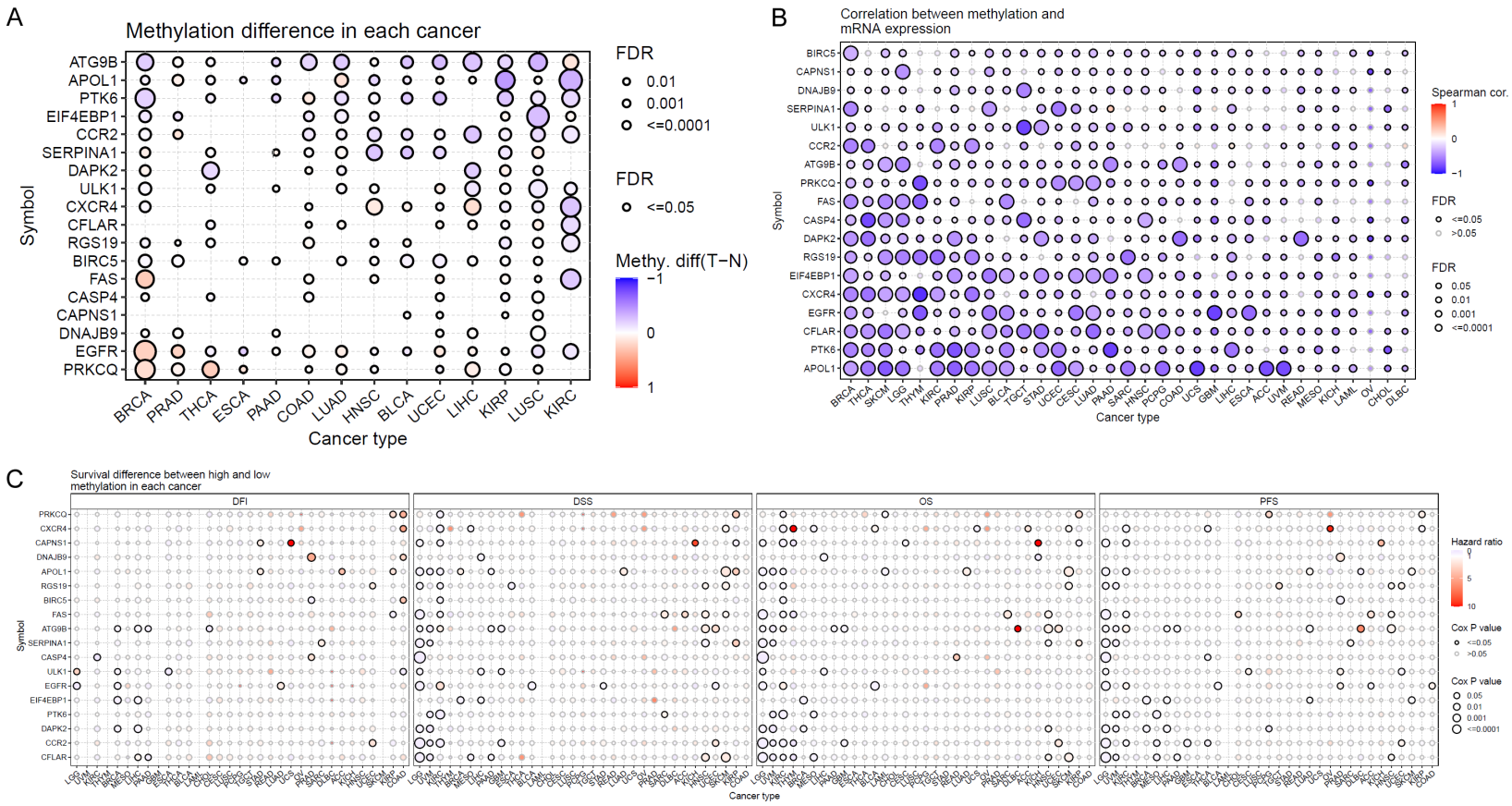
A
Methylation difference in each cancer
Symbol
ATG9B
APOL1
PTK6
EIF4EBP1
CCR2
SERPINA1
DAPK2
ULK1
CXCR4
CFLAR
RGS19
BIRC5
FAS
CASP4
CAPNS1
DNAJB9
EGFR
PRKCQ
BRCA PRAD THCA ESCA PAAD COAD LUAD HNSC BLCA UCEC LIHC KIRP LUSC KIRC
Cancer type
FDR
0.01
0.001
<=0.0001
FDR
<=0.05
Methy. diff(T−N)
1
0
−1
B
Correlation between methylation and mRNA expression
Symbol
BIRC5
CAPNS1
DNAJB9
SERPINA1
ULK1
CCR2
ATG9B
PRKCQ
FAS
CASP4
DAPK2
RGS19
EIF4EBP1
CXCR4
EGFR
CFLAR
PTK6
APOL1
BRCA THCA SKCM LGG THYM KIRC PRAD KIRP LUSC BLCA TGCT STAD UCEC CESC LUAD PRAD SARC HNSC PCPG COAD UCS GBM LIHC ESCA ACC UVM READ MESO KICH LAML OV CHOL DLBC
Cancer type
Spearman cor.
1
0
−1
FDR
<=0.05
>0.05
FDR
0.05
0.01
0.001
<=0.0001
C
Survival difference between high and low methylation in each cancer
DFI
DSS
OS
PFS
Symbol
PRKCQ
CXCR4
CAPNS1
DNAJB9
APOL1
RGS19
BIRC5
FAS
ATG9B
SERPINA1
CASP4
ULK1
EGFR
EIF4EBP1
PTK6
DAPK2
CCR2
CFLAR
Cancer type
Hazard ratio
0
5
10
Cox P value
<=0.05
>0.05
Cox P value
0.05
0.01
0.001
<=0.0001

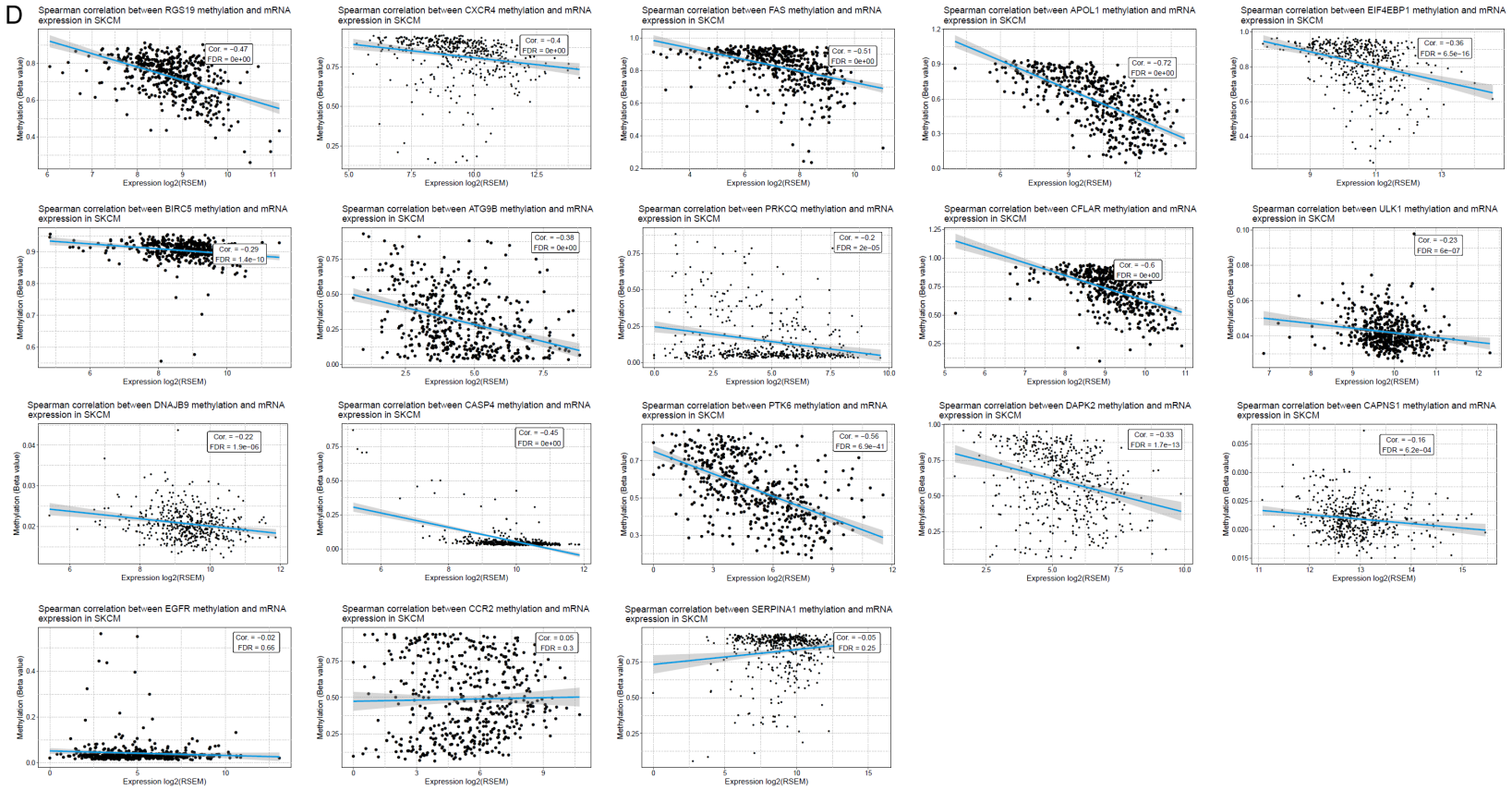

Figure S4. Methylation analysis of the 18 DE-ARGs. A. Methylation difference in each cancer. B. The correlation between the 18 DE-ARGs' methylation and their corresponding mRNA expression in pan-cacners. C. The analysis of survival difference including OS, PFS, DSS and DFI between high and low methylation in pan-cancers. D. The correlation of the 18 DE-ARGs methylation and their corresponding mRNA expression in SKCM.

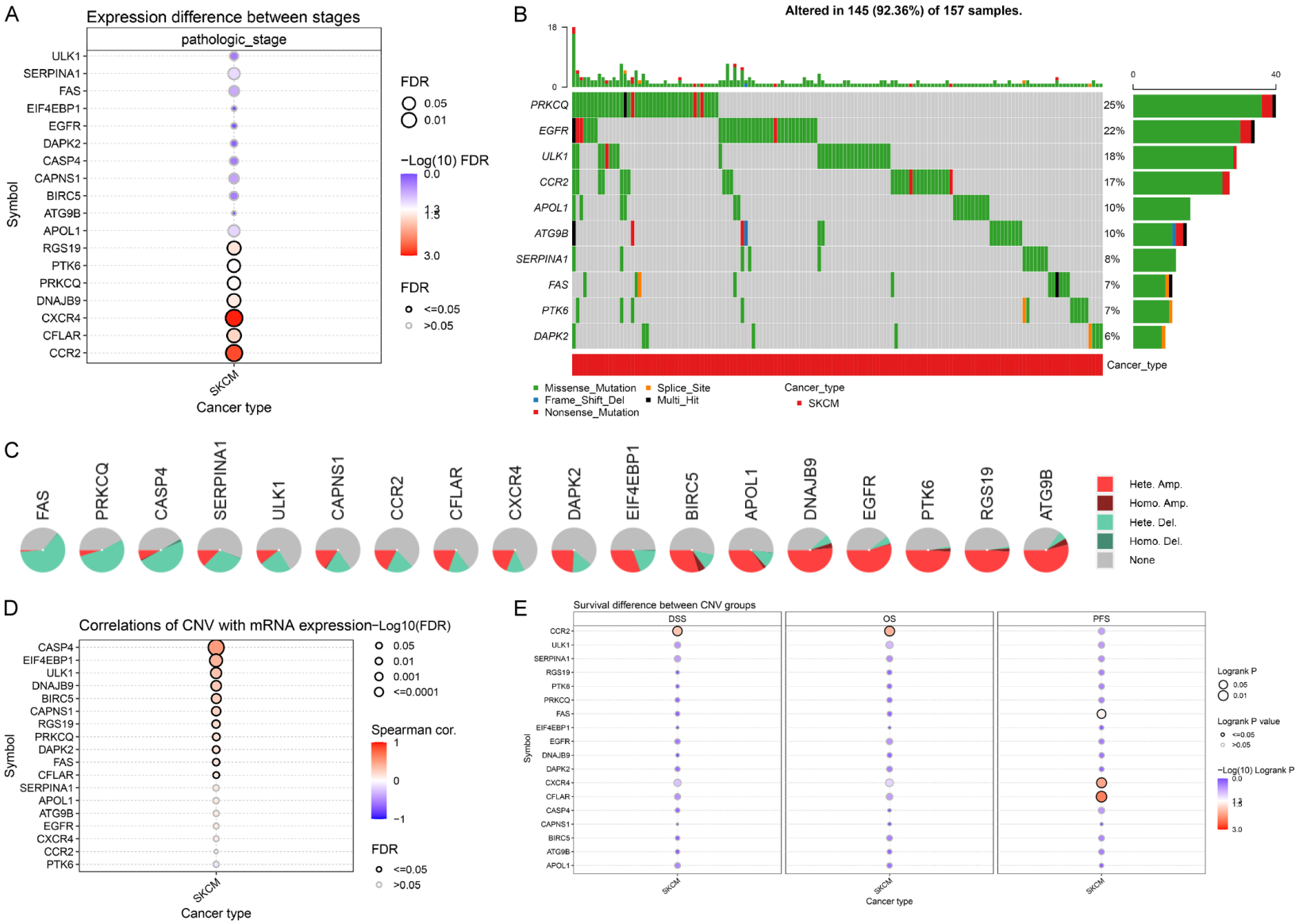
A
Expression difference between stages
pathologic_stage
ULK1
SERPINA1
FAS
EIF4EBP1
EGFR
DAPK2
CASP4
CAPNS1
BIRC5
ATG9B
APOL1
RGS19
PTK6
PRKCQ
DNAJB9
CXCR4
CFLAR
CCR2
Symbol
SKCM
Cancer type
FDR
0.05
0.01
−Log(10) FDR
0.0
1.3
1.5
3.0
FDR
<=0.05
>0.05
B
Altered in 145 (92.36%) of 157 samples.
18
0
0
40
PRKCQ 25%
EGFR 22%
ULK1 18%
CCR2 17%
APOL1 10%
ATG9B 10%
SERPINA1 8%
FAS 7%
PTK6 7%
DAPK2 6%
Cancer_type
Missense_Mutation
Frame_Shift_Del
Nonsense_Mutation
Splice_Site
Multi_Hit
Cancer_type
SKCM
C
FAS
PRKCQ
CASP4
SERPINA1
ULK1
CAPNS1
CCR2
CFLAR
CXCR4
DAPK2
EIF4EBP1
BIRC5
APOL1
DNAJB9
EGFR
PTK6
RGS19
ATG9B
Hete. Amp.
Homo. Amp.
Hete. Del.
Homo. Del.
None
D
Correlations of CNV with mRNA expression−Log10(FDR)
CASP4
EIF4EBP1
ULK1
DNAJB9
BIRC5
CAPNS1
RGS19
PRKCQ
DAPK2
FAS
CFLAR
SERPINA1
APOL1
ATG9B
EGFR
CXCR4
CCR2
PTK6
Symbol
SKCM
Cancer type
0.05
0.01
0.001
<=0.0001
Spearman cor.
1
0
−1
FDR
<=0.05
>0.05
E
Survival difference between CNV groups
DSS
OS
PFS
CCR2
ULK1
SERPINA1
RGS19
PTK6
PRKCQ
FAS
EIF4EBP1
EGFR
DNAJB9
DAPK2
CXCR4
CFLAR
CASP4
CAPNS1
BIRC5
ATG9B
APOL1
Symbol
SKCM
SKCM
SKCM
Cancer type
Logrank P
0.05
0.01
Logrank P value
<=0.05
>0.05
−Log(10) Logrank P
0.0
1.3
1.5
3.0

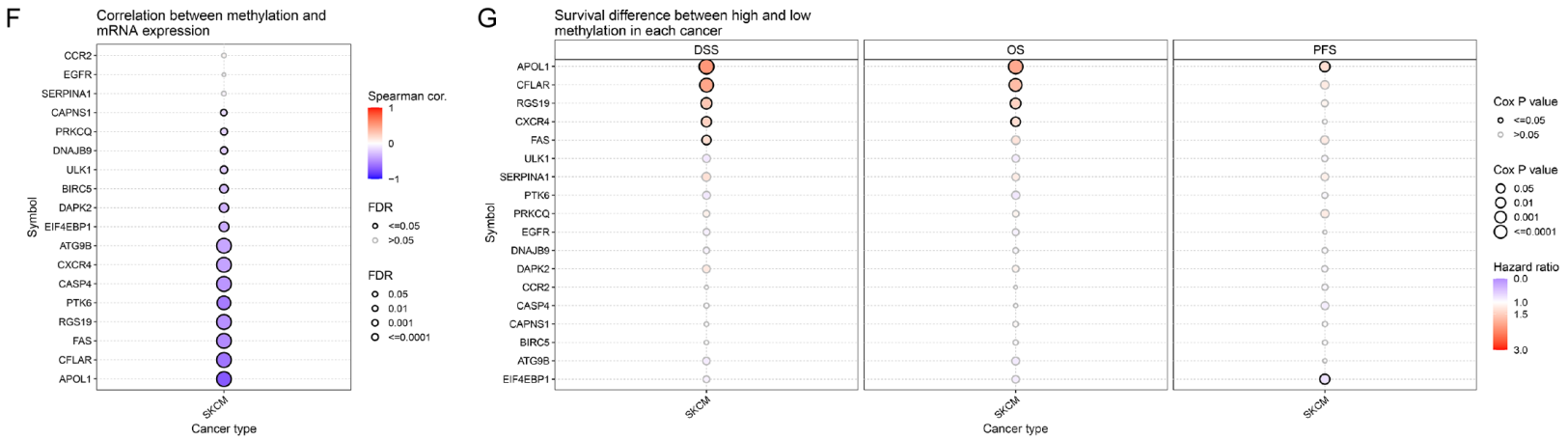

Figure S5. SNV, CNV and methylation analysis of 18 DE-ARGs in SKCM. A. The expression difference of the 18 DE-ARGs between pathologic stages in SKCM. B. The waterfall plot displayed the top 10 mutated genes in SKCM. C. The CNV analysis of 18 DE-ARGs in SKCM. D. The correlations between CNV and mRNA expression of all the 18 DE-ARGs. E. The survival difference including OS, PFS and DSS, between CNV groups. F. The correlation between methylation and 18 DE-ARGs mRNA expression in SKCM. G. The survival difference including OS, PFS and DSS, between methylation high or low groups.

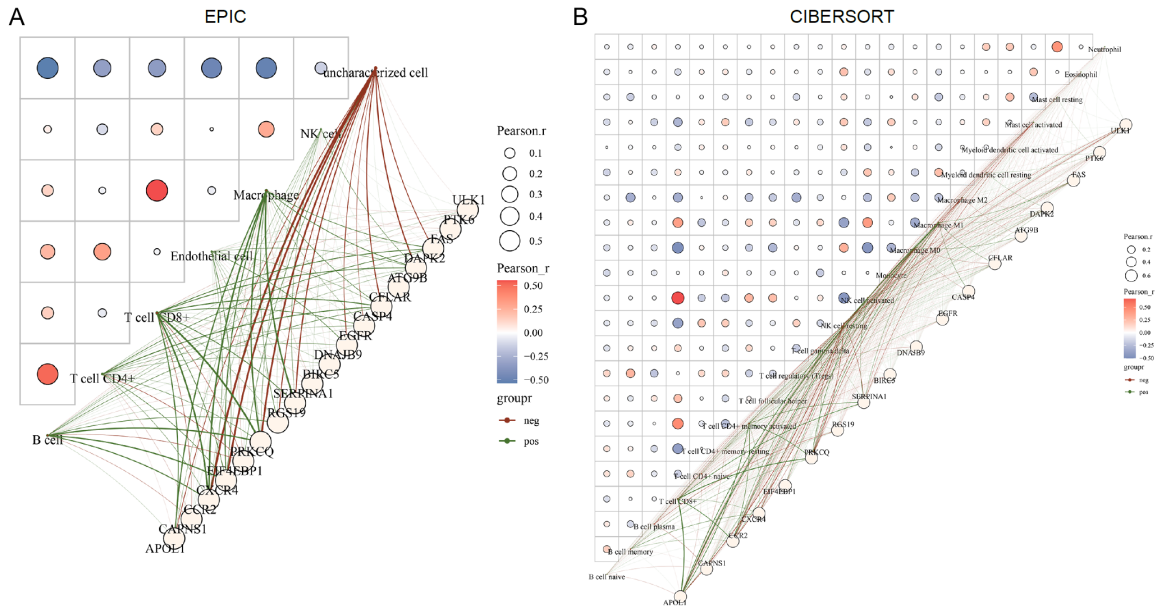

Figure S6. Immune interacting network construction using 18 DE-ARGs in SKCM. A. Immune interacting network construction using EPIC algorithm. B. Immune interacting network construction using CIBERSORT algorithm.

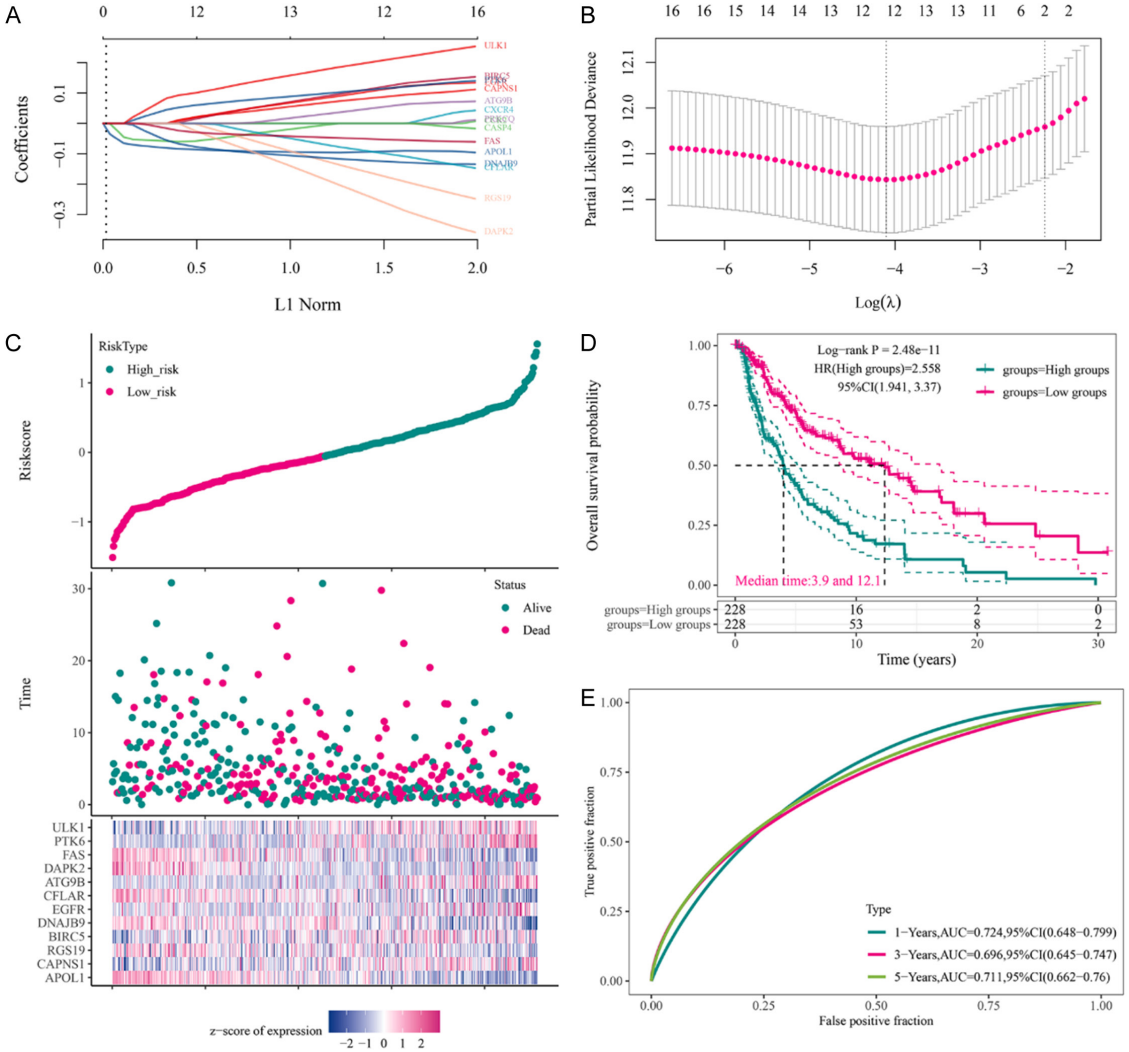

Figure S7. Constructing a prognostic signature using DE-ARGs. A. LASSO coefficients profiles of 18 DE-ARGs. LASSO: the least absolute shrinkage and selection operator. B. LASSO regression with tenfold cross-validation obtained 10 prognostic genes using minimum log (λ) value. C. Heatmap of the curve of risk score, survival status and expression profiles of the 12 prognostic signature genes in high-risk and low-risk subgroup in SKCM. D. Overall survival analysis of high- and low-subgroup in SKCM. E. The ROC analysis of the 12-genes prognostic signature for predicting the 1-, 3-, 5-year overall survival in SKCM.

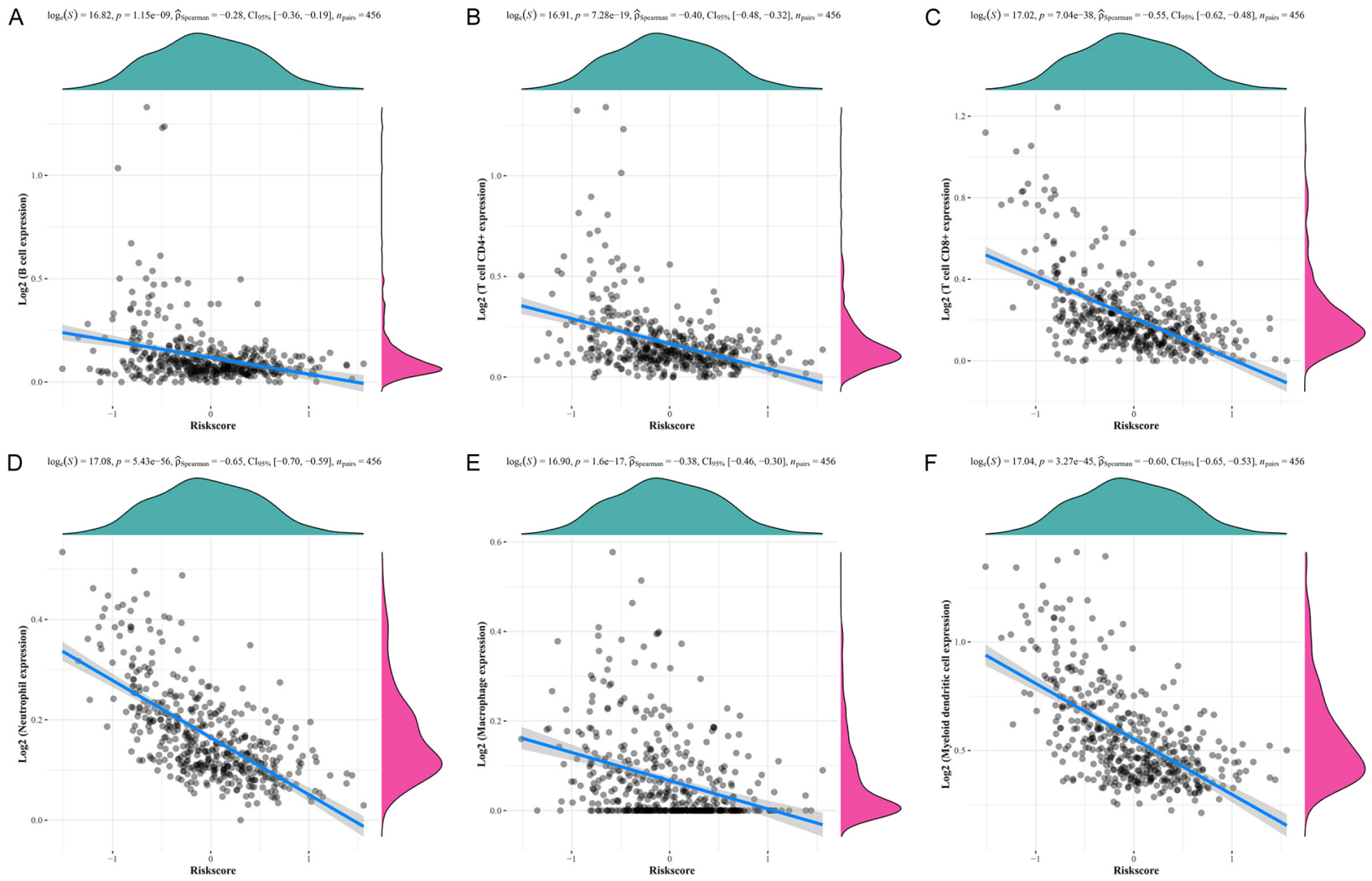

Figure S8. The correlation analysis between 12-ARGs prognostic signature and immune infiltration cell types. A. B cell. B. CD4+ T cell. C. CD8+ T cell. D. Neutrophil. E. Macrophage. F. Myeloid dendritic cell.

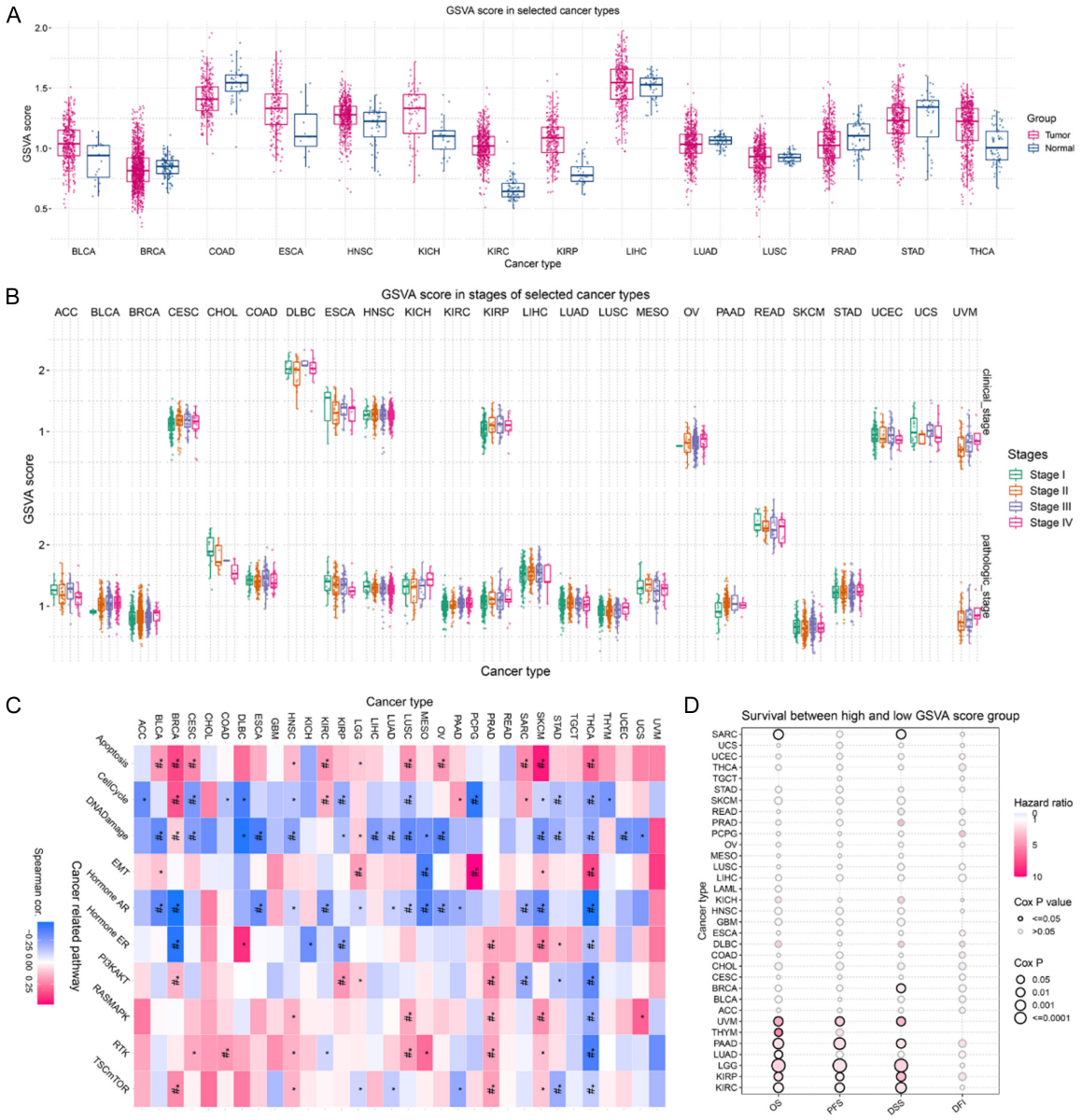

Figure S9. GSVA analysis in pan-cancers. A. Gene Set Variation Analysis (GSVA) score in tumor and normal tissue samples across TCGA cancer types. The 12 prognostic signature genes was used as a whole gene set to evaluate the GSVA score. B. The GSVA score analysis in clinical- and pathologic-stages (stage I, II, III and IV) of TCGA cancer types. C. The relationship between kinds of signaling pathway activity and the GSVA score. D. The survival analysis of the high and low GSVA score.

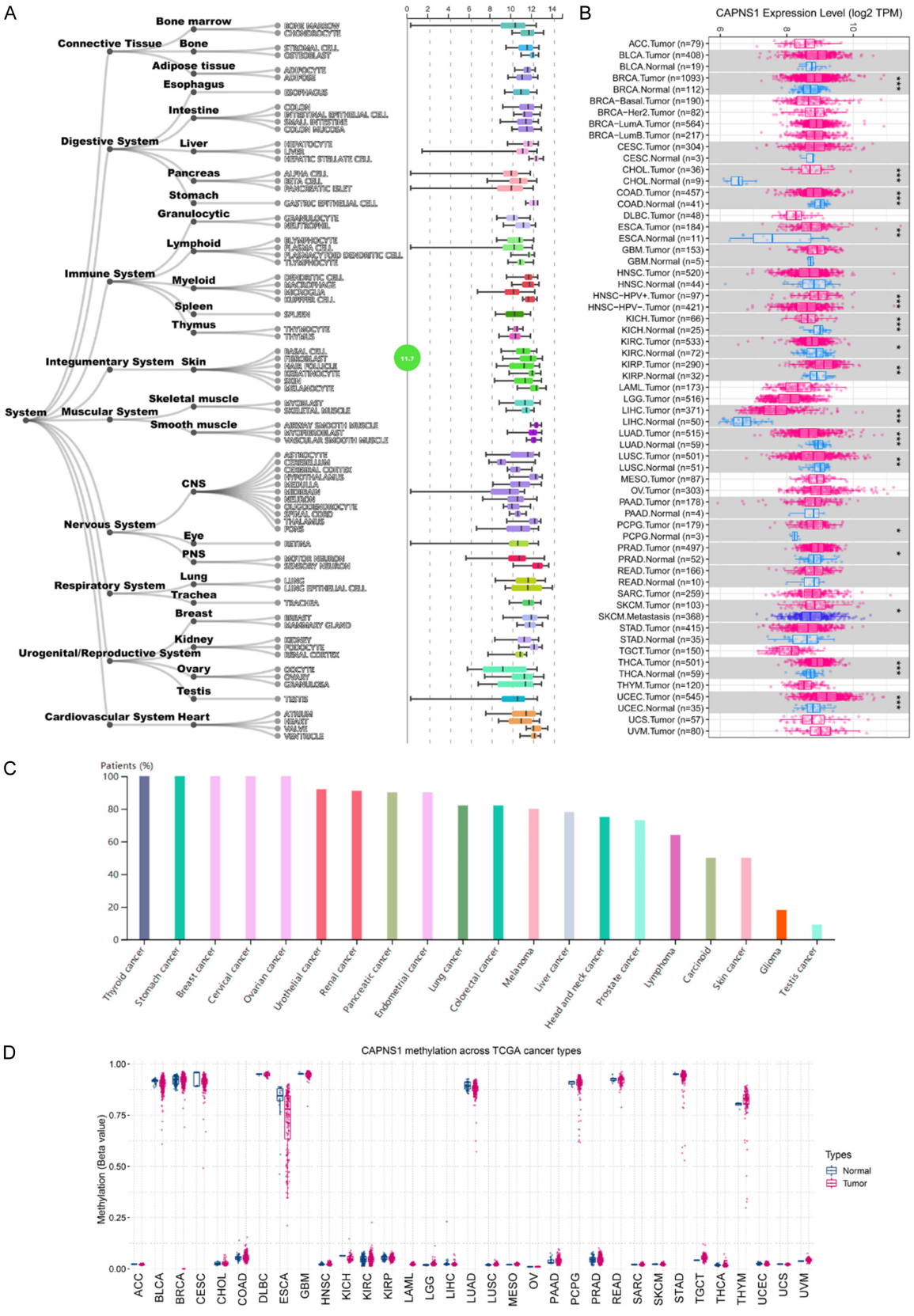

Figure S10. The expression and methylation analysis of CAPNS1. A. The CAPNS1 expression in numerous normal tissues and cells using Harmonizome 3.0 database. B. The CAPNS1 expression levels in pan-cancers. C. The protein levels of CAPNS1 in kinds of cancer types. D. The CAPNS1 methylation levels across TCGA cancer types.

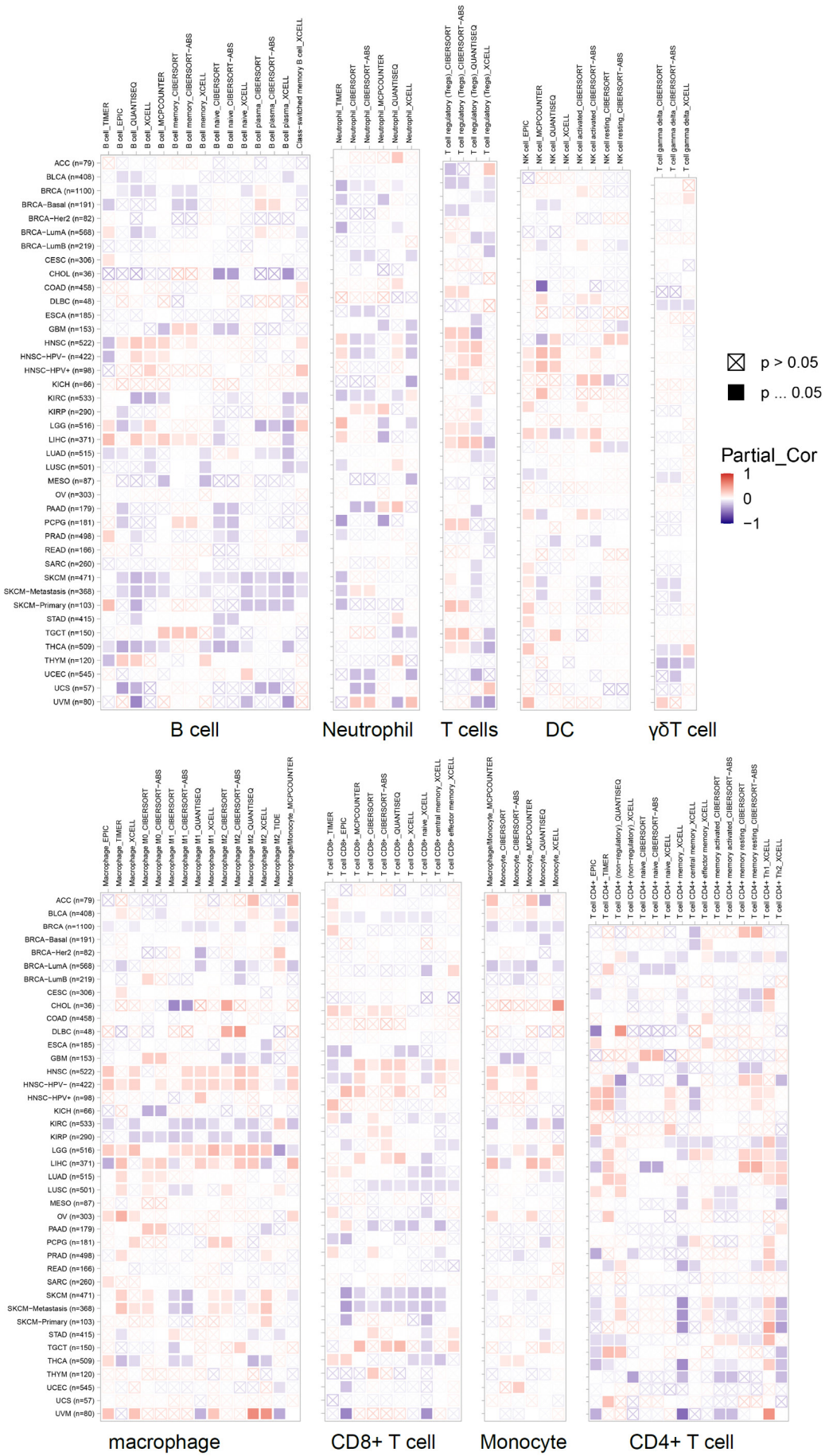
B cell_TIMER
B cell_EPIC
B cell_QUANTISEQ
B cell_XCELL
B cell_MCPCOUNTER
B cell memory_CIBERSORT
B cell memory_CIBERSORT-ABS
B cell memory_XCELL
B cell naive_CIBERSORT
B cell naive_CIBERSORT-ABS
B cell naive_XCELL
B cell plasma_CIBERSORT
B cell plasma_CIBERSORT-ABS
B cell plasma_XCELL
Class-switched memory B cell_XCELL
Neutrophil_TIMER
Neutrophil_CIBERSORT
Neutrophil_CIBERSORT-ABS
Neutrophil_MCPCOUNTER
Neutrophil_QUANTISEQ
Neutrophil_XCELL
T cell regulatory (Tregs)_CIBERSORT
T cell regulatory (Tregs)_CIBERSORT-ABS
T cell regulatory (Tregs)_QUANTISEQ
T cell regulatory (Tregs)_XCELL
NK cell_EPIC
NK cell_MCPCOUNTER
NK cell_QUANTISEQ
NK cell_XCELL
NK cell activated_CIBERSORT
NK cell activated_CIBERSORT-ABS
NK cell resting_CIBERSORT
NK cell resting_CIBERSORT-ABS
T cell gamma delta_CIBERSORT
T cell gamma delta_CIBERSORT-ABS
T cell gamma delta_XCELL
ACC (n=79)
BLCA (n=408)
BRCA (n=1100)
BRCA−Basal (n=191)
BRCA−Her2 (n=82)
BRCA−LumA (n=568)
BRCA−LumB (n=219)
CESC (n=306)
CHOL (n=36)
COAD (n=458)
DLBC (n=48)
ESCA (n=185)
GBM (n=153)
HNSC (n=522)
HNSC−HPV− (n=422)
HNSC−HPV+ (n=98)
KICH (n=66)
KIRC (n=533)
KIRP (n=290)
LGG (n=516)
LIHC (n=371)
LUAD (n=515)
LUSC (n=501)
MESO (n=87)
OV (n=303)
PAAD (n=179)
PCPG (n=181)
PRAD (n=498)
READ (n=166)
SARC (n=260)
SKCM (n=471)
SKCM−Metastasis (n=368)
SKCM−Primary (n=103)
STAD (n=415)
TGCT (n=150)
THCA (n=509)
THYM (n=120)
UCEC (n=545)
UCS (n=57)
UVM (n=80)
B cell
Neutrophil
T cells
DC
γδT cell
p > 0.05
p ... 0.05
Partial_Cor
1
0
−1
Macrophage_EPIC
Macrophage_TIMER
Macrophage_XCELL
Macrophage M0_CIBERSORT
Macrophage M0_CIBERSORT-ABS
Macrophage M1_CIBERSORT
Macrophage M1_CIBERSORT-ABS
Macrophage M1_QUANTISEQ
Macrophage M1_XCELL
Macrophage M2_CIBERSORT
Macrophage M2_CIBERSORT-ABS
Macrophage M2_QUANTISEQ
Macrophage M2_XCELL
Macrophage M2_TIDE
Macrophage/Monocyte_MCPCOUNTER
T cell CD8+_TIMER
T cell CD8+_EPIC
T cell CD8+_MCPCOUNTER
T cell CD8+_CIBERSORT
T cell CD8+_CIBERSORT-ABS
T cell CD8+_QUANTISEQ
T cell CD8+_XCELL
T cell CD8+ naive_XCELL
T cell CD8+ central memory_XCELL
T cell CD8+ effector memory_XCELL
Macrophage/Monocyte_MCPCOUNTER
Monocyte_CIBERSORT
Monocyte_CIBERSORT-ABS
Monocyte_MCPCOUNTER
Monocyte_QUANTISEQ
Monocyte_XCELL
T cell CD4+_EPIC
T cell CD4+_TIMER
T cell CD4+ (non−regulatory)_QUANTISEQ
T cell CD4+ (non−regulatory)_XCELL
T cell CD4+ naive_CIBERSORT
T cell CD4+ naive_CIBERSORT-ABS
T cell CD4+ naive_XCELL
T cell CD4+ memory_XCELL
T cell CD4+ central memory_XCELL
T cell CD4+ effector memory_XCELL
T cell CD4+ memory activated_CIBERSORT
T cell CD4+ memory activated_CIBERSORT-ABS
T cell CD4+ memory resting_CIBERSORT
T cell CD4+ memory resting_CIBERSORT-ABS
T cell CD4+ Th1_XCELL
T cell CD4+ Th2_XCELL
macrophage
CD8+ T cell
Monocyte
CD4+ T cell

Figure S11. Immune cell infiltration analysis of CAPNS1 in pan-cancers. The immune cells included B cell, CD4+ T cell, CD8+ T cell, Neutrophil, Macrophage, Myeloid DC, NK cell, T cell, γδT cell, monocyte.

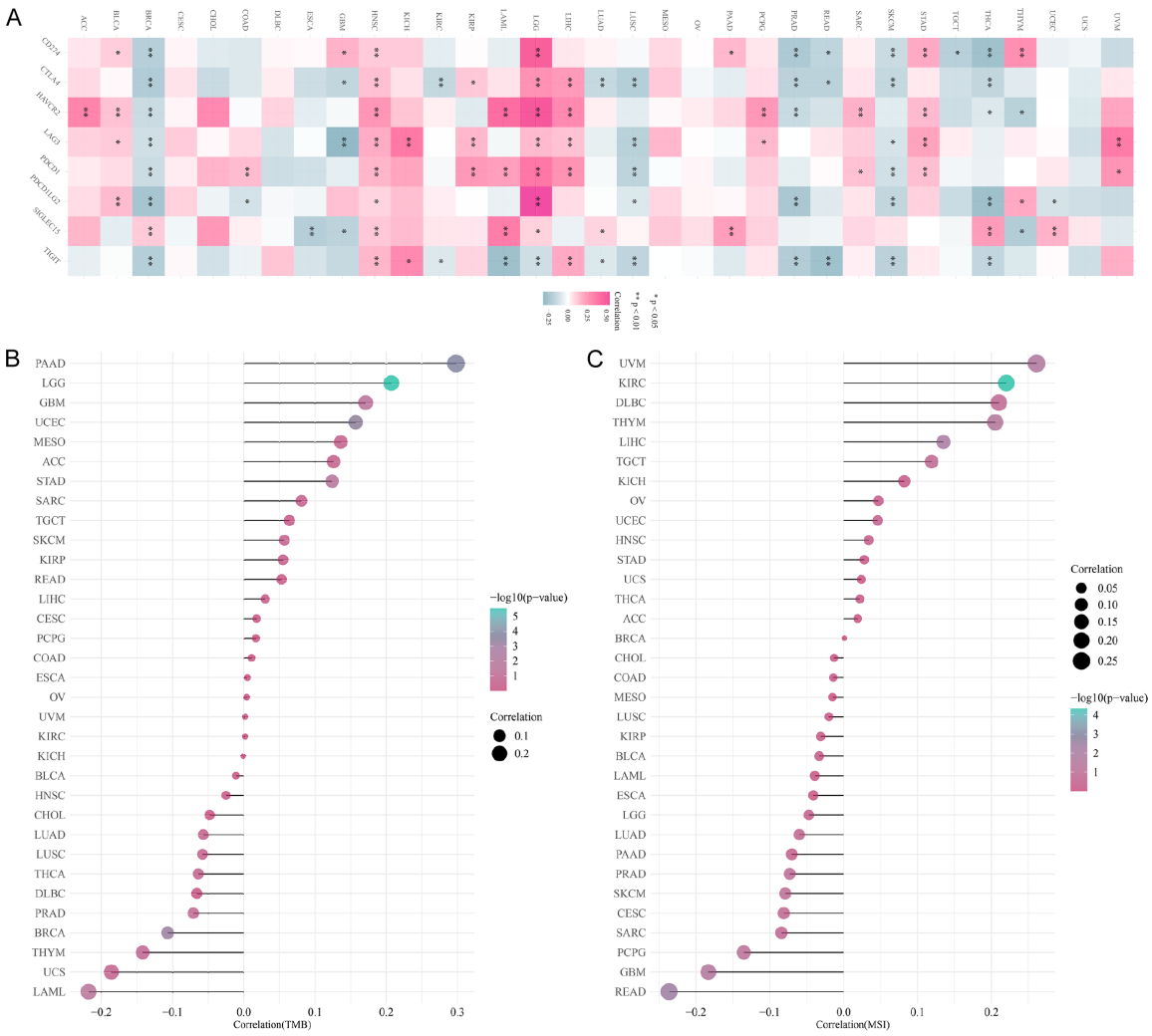

Figure S12. The immune checkpoints, TMB and MSI analyses of CAPNS1 in pan-cancers. A. The correlation between CAPNS1 expression and the immune checkpoints. B. The correlation of CAPNS1 and TMB (tumor mutation burden) in pan-cancers. C. The correlation of CAPNS1 and MSI (microsatellite instability) in pan-cancers.

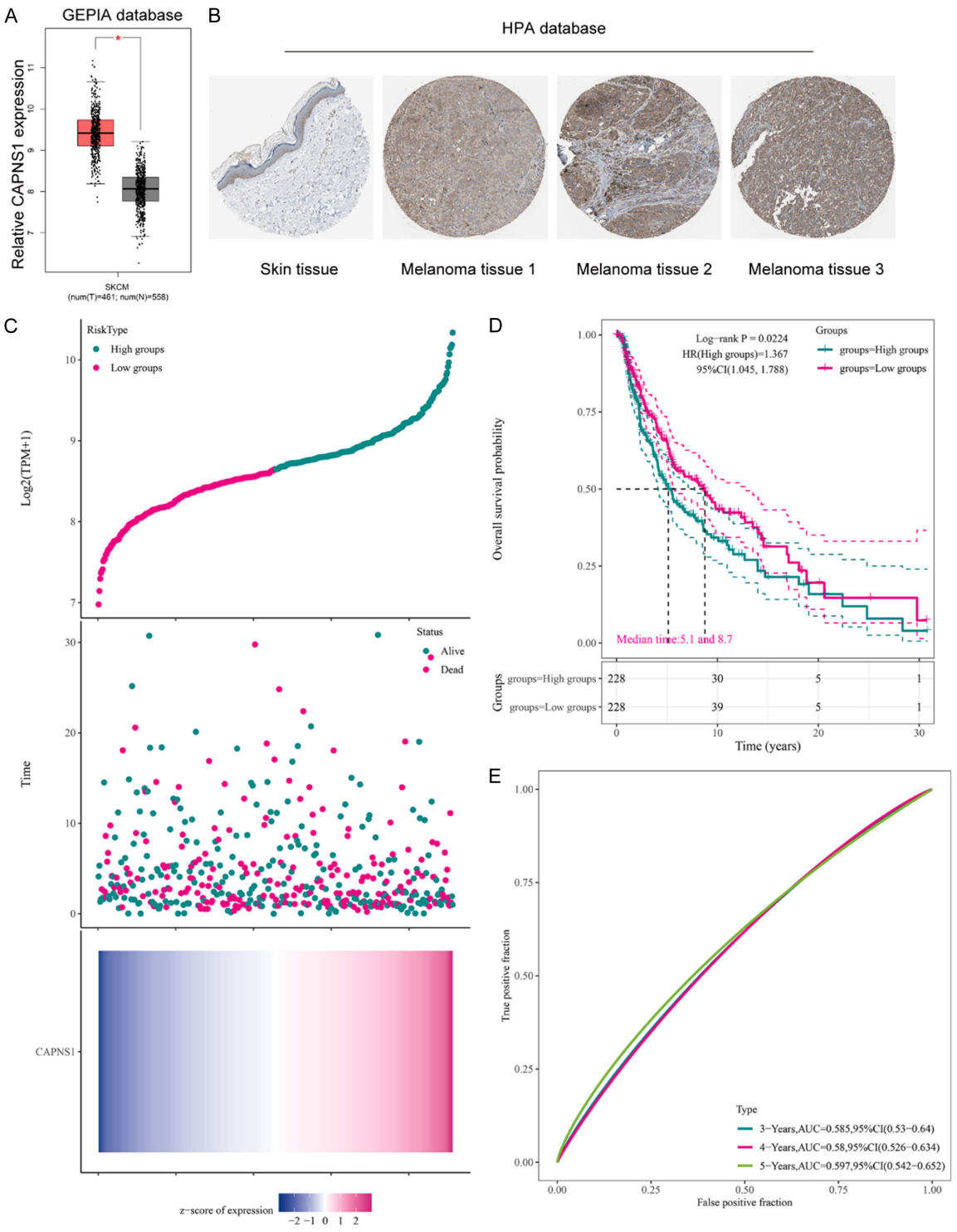

Figure S13. CAPNS1 might be a prognostic signature in SKCM. A. The relative CAPNS1 expression in SKCM samples. Since the TCGA-SKCM data had no control normal tissues of SKCM, the 588 normal tissue samples from GTEx database were used as control. B. The immunohistochemistry analyses of CAPNS1 in melanoma tumor tissues and normal skin tissues from HPA database. C. A heatmap depicting the curve of risk score, survival status, and expression patterns of CAPNS1 in the high-risk and low-risk subgroups of SKCM patient. D. Overall survival analysis of CAPNS1 high- and low-subgroup in SKCM. E. The ROC analysis of CAPNS1 for predicting the 3-, 4-, 5-year overall survival in SKCM. ROC: receiver operating characteristic; AUC: area under the ROC curve.

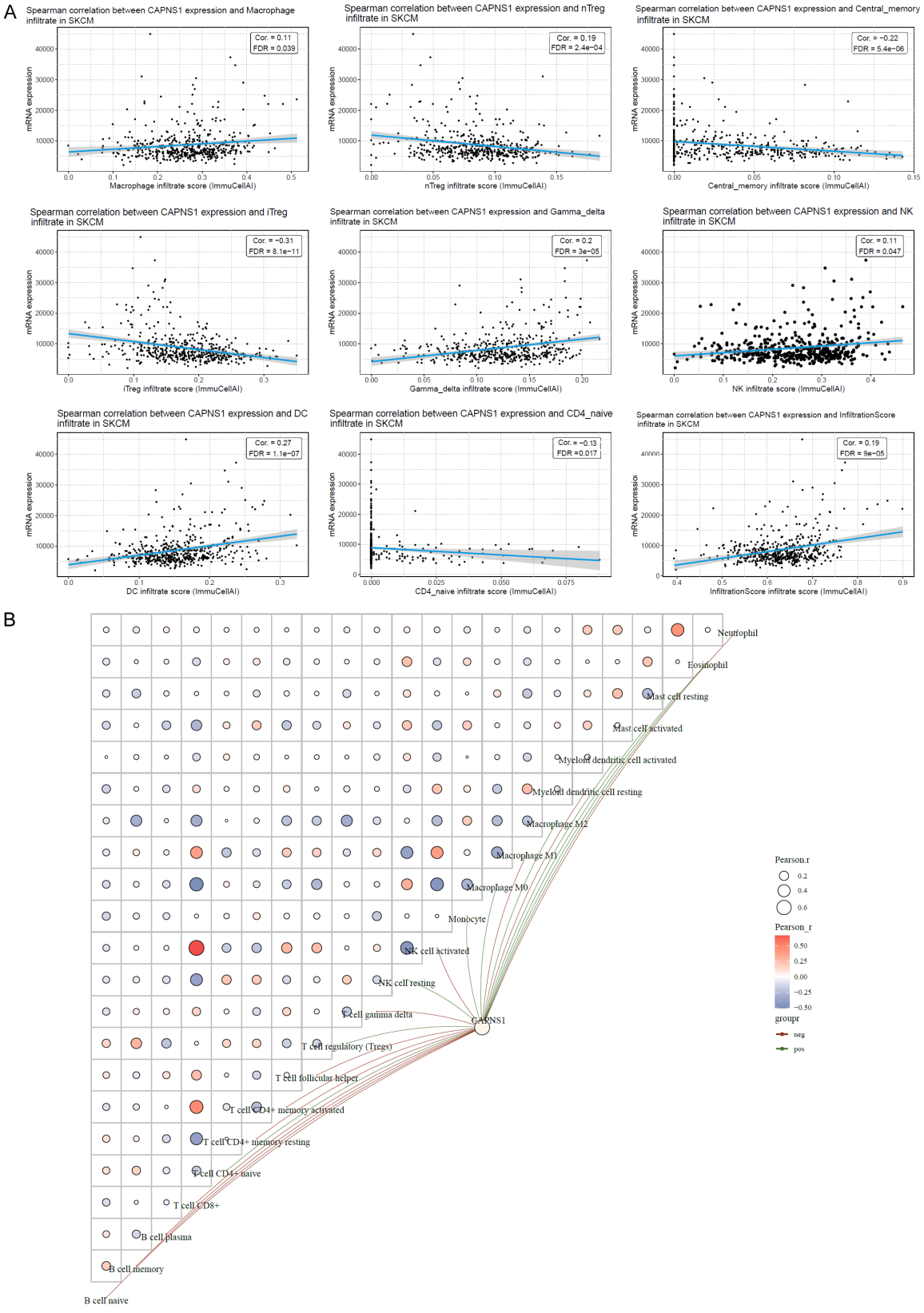

Figure S14. The immune interacting network between CAPNS1 and immune infiltration. A. The correlation CAPNS1 and different immune cells infiltration in SKCM, including NK, γδT cell, macrophage, DC, infiltration score, nTreg, central memory infiltration, iTreg, CD4 naive infiltration. B. The immune interacting network between CAPNS1 and kinds of immune cells in SKCM.

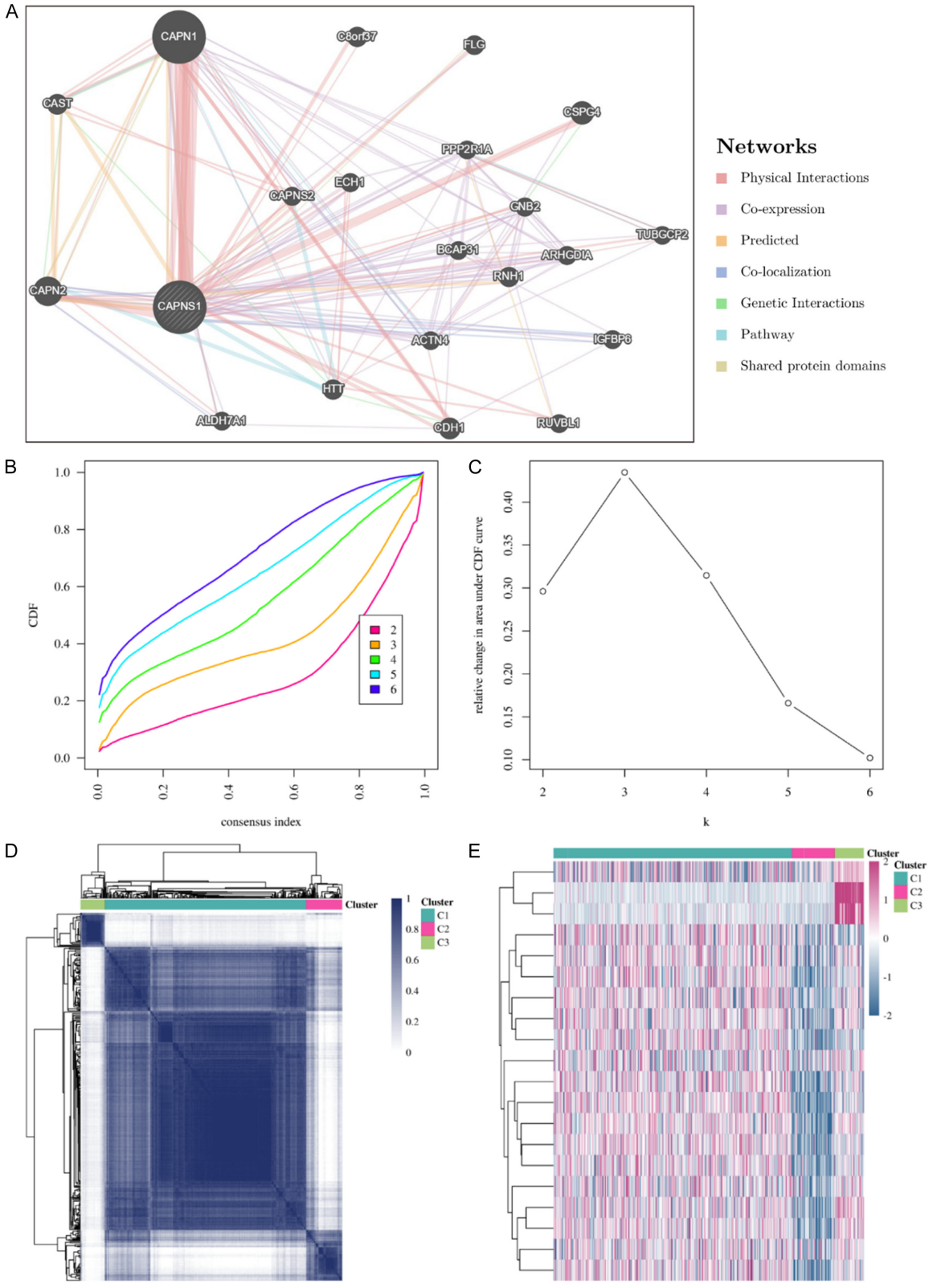

Figure S15. Molecular subtypes identification in SKCM based on CAPNS1 interacting genes. A. The interacting network of CAPNS1 generated by using Genemania database. B. The cumulative distribution function (CDF) curves (k = 2, 3, 4, 5, and 6) in consensus cluster analysis. C. Relative change in area under the CDF curve when k = 2-6. D. The heatmap related to the consensus matrix for k = 3. E. The heatmap of deferentially expressed genes in the three sub-groups. Group 1 (C1), group 2 (C2) and group 3 (C3) respectively contained 362, 65 and 44 SKCM samples.